

# **Perturbation Estimation Based Nonlinear Adaptive Power Decoupling Control for DFIG Wind Turbine**

Kai Shi, Xin Yin, Lin Jiang, Member, IEEE, Yang Liu, Yihua Hu, Senior Member, Huiqing Wen,  
Member IEEE

## **List of authors:**

**Kai Shi, Xin Yin, Lin Jiang, Yihua Hu** are with the Department of Electrical Engineering and  
Electronics, University of Liverpool, Liverpool, United Kingdom, L69 3GJ

**Yang Liu** is with the School of Electric Power Engineering, South China University of Technology,  
Guangzhou, China, 510640.

**Huiqing Wen** is with the Department of Electrical Engineering and Electronics, Xi'an Jiaotong-  
Liverpool University, Suzhou, China

Corresponding author:

Dr. Lin Jiang

Department of Electrical Engineering & Electronics

University of Liverpool

Liverpool, UK, L69 3GJ

Tel: +44 - 151 794 4509

Email: [ljiang@liv.ac.uk](mailto:ljiang@liv.ac.uk)

**Abstract** – This paper proposes a perturbation estimation based nonlinear adaptive power decoupling controller for doubly-fed induction generator based wind turbines (DFIG-WTs). Perturbation states are defined to include the nonlinearities, uncertainties of the system model, the cross-coupling between control loops, and external disturbances. Perturbation observers are designed to estimate the fast time-varying perturbation states. With perturbation estimation, the DFIG-WT system is fully decoupled, and an output feedback control can be designed for the control of rotor currents. Rotor current references are calculated based on the steady-state relation between active/reactive power and rotor current, and stator dynamic is ignored. The performance of the proposed controller is evaluated and verified via both simulation and experimental tests.

**Index Terms** – DFIG-WT, power decoupled control, perturbation estimation, nonlinear adaptive control.

## NOMENCLATURE

$v_{ds}, v_{qs}$	The $d$ -axis and $q$ -axis components of stator voltage, respectively.
$v_{dr}, v_{qr}$	The $d$ -axis and $q$ -axis components of rotor voltage, respectively.
$i_{ds}, i_{qs}$	The $d$ -axis and $q$ -axis components of stator current, respectively.
$i_{dr}, i_{qr}$	The $d$ -axis and $q$ -axis components of rotor current, respectively.
$R_s, R_r$	Stator and rotor winding resistances, respectively.
$L_s, L_r, L_m$	Stator, rotor, and mutual inductances, respectively.
$P_s, Q_s$	Stator active and reactive power outputs.
$\omega_s, \omega_r, \omega_m$	Synchronous frequency, rotor electrical speed, rotor mechanical speed, respectively.
$P_s^*, Q_s^*$	Reference values of stator active and reactive power outputs, respectively.
$i_{dr}^*, i_{qr}^*$	Reference values of the $d$ -axis and $q$ -axis components of rotor current, respectively.
$v_{dr}^*, v_{qr}^*$	Reference values of the $d$ -axis and $q$ -axis components of rotor voltage, respectively.
$k_d, k_q$	Feedback control gains.
$h_{d1}, h_{d2}, h_{q1}, h_{q2}$	Perturbation observer gains.

## I. INTRODUCTION

The amount of wind power penetration into power grids keeps increasing in the past decade. The DFIG-WT is featured by that the capacity of its converters is only one-third of a full-scale wind power generator. The typical topology of a DFIG-WT is shown in Fig.1, in which the stator windings are directly connected to the grid, and the rotor windings are fed to the grid by back-to-back converters [1]. The PWM controlled back-to-back converters allow bidirectional power flow between the grid and rotor windings. In normal operation, the grid-side converter (GSC) is controlled to maintain a constant DC-link voltage and generate

a specific amount of reactive power, and the rotor-side converter (RSC) is controlled to regulate the power outputs of stator windings by feeding proper voltages into rotor windings. With different control strategies, DFIG-WT can achieve various control targets such as maximum power point tracking (MPPT) [2], frequency regulation [3], reactive power control [4], and voltage control [5], etc.

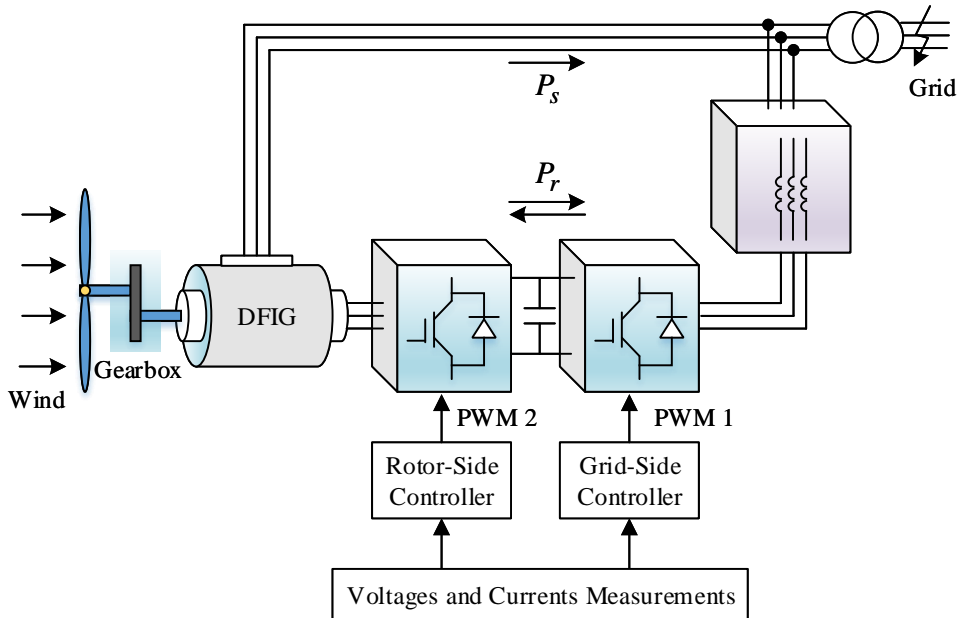


**Fig. 1 Grid-connected DFIG-WT with back-to-back converters [1]**

Conventional vector control (VC) [6] has been widely used in DFIG-WTs, via decoupling the rotor currents into d- and q-axis components in the synchronous rotational frame, which is either stator flux oriented [7], [8], or stator voltage oriented [9], [10]. Then the active and reactive powers can be controlled by regulating d- and q-axis rotor currents separately. The conventional VC has advantages of low total harmonic distortion (THD), high precision, and low switching frequency [11]; while it also shows drawbacks in the following aspects. First, the conventional VC is model-based which makes it sensitive to parameter variations [12]. Moreover, the conventional VC is an asymptotic decoupling control with PI controllers; its performance may get worse when system operation point changes [13], [14]. Furthermore, conventional VC is realized based on the assumption of a strong external power grid and the neglect of stator resistance, which cannot be satisfied during the transient processes of grid disturbances [15]-[18].

To improve the transient performance of DFIGs, direct power/torque control and advanced nonlinear control strategies have been proposed. The direct power/torque control methods of DFIGs are achieved by directly controlling the scalar variables, which include active/reactive power and torque variables [19]-[22]. Nonlinear control methods such as sliding-mode control [14], back-stepping control [23], differential flatness based control [24], and feedback linearization control (FLC) [25], etc., have also been applied in the control of DFIGs. The control of DFIGs can be performed using cascade structure that is same as the conventional VC but with improved inner-loop current controllers, such as hysteresis-based controllers

[26], [27], feedback linearizing control (FLC) [28], [29], and other controllers designed for fault ride-through (FRT) enhancement [30]-[36]. The FLC theory allows exact linearization and fully decoupling of the nonlinear system such that linear feedback control law can be applied [37]. However, the reliance on full-state feedback and the requirement of accurate system model make the FLC present poor robustness to parameter uncertainties. Practically, the rotor resistance of the DFIG is varied due to the change of temperature and the use of power electronics converters. The values of inductance are obtained via parameter estimation processes, which risk the control performance by using mismatched parameters in controllers. To remedy the drawbacks of FLC, disturbance observer based FLC (DOFLC) has been proposed in [28], in which a disturbance observer is used to estimate system uncertainties and disturbances. However, the controller in [28] can only handle the unknown constant or slow time-varying disturbance and the disturbance observer used is proposed by [45] with detailed analysis. The previous research suggests that the perturbation estimation-based nonlinear control is able to provide real-time compensation of fast time-varying disturbances and has a control structure that is simpler than other nonlinear controllers [39], [40]. Furthermore, the characteristics of those disturbance observer based controllers are reviewed in [38].

This paper proposes a perturbation estimation based nonlinear adaptive power decoupling controller for DFIG-WTs. Different from the controller in [40], which is a four-loop controller, the proposed controller only considers rotor transients and neglects the stator transients. The rotor current references are calculated from the power references based on their steady-state relationship. High-gain perturbation observer is designed to estimate system perturbations, including system cross-couplings, nonlinearities, un-modelled dynamics, and external disturbance. An output feedback controller is designed for the linearized system. Both simulation and experiment studies have been carried out to evaluate the improved performance of proposed controller in comparison with the conventional VC and the controller presented in [28].

## **II. PERTURBATION ESTIMATION BASED NONLINEAR ADAPTIVE POWER DECOUPLING CONTROLLER FOR GRID-CONNECTED DFIG-WT**

The proposed controller generates rotor voltage reference values that are required to be injected into rotor windings via PWM converters such that the d- and q- axis rotor currents are able to track their references. The references of rotor currents are calculated based on the active power and reactive power commands at steady state. Hence, the decoupled control of active/reactive powers can be achieved via controlling the corresponding components of rotor currents. As the speed control is usually required by DFIG-WTs in real operation, an outer speed loop is implemented in cascade with the current control loops to calculate the active power reference [41].

The inner current dynamic systems are decoupled and linearized by compensating the perturbations which are defined to include all system nonlinearities, interactions between the d-axis and the q-axis loop,

and external disturbances. A perturbation observer is designed for each subsystem to estimate the system perturbations.

This section presents the model of DFIG-WT at first, followed by the configuration of the control framework with proposed controller. Then, the input-output linearization of the rotor current dynamics is presented. Finally, the design of perturbation observers and the synthesis of control inputs with the proposed controller are presented.

### A. Modelling of the DFIG-WT

The dynamic equations of the DFIG stator and rotor currents in the synchronous  $dq$  reference frame can be written as [28], [42]:

$$\begin{cases} \frac{di_{ds}}{dt} = -\frac{R_s}{\sigma L_s} i_{ds} + \left( \omega_s + \frac{\omega_r L_m^2}{\sigma L_s L_r} \right) i_{qs} + \frac{R_r L_m}{\sigma L_s L_r} i_{dr} + \frac{\omega_r L_m}{\sigma L_s} i_{qr} + \frac{1}{\sigma L_s} v_{ds} - \frac{L_m}{\sigma L_s L_r} v_{dr} \\ \frac{di_{qs}}{dt} = -\left( \omega_s + \frac{\omega_r L_m^2}{\sigma L_s L_r} \right) i_{ds} - \frac{R_s}{\sigma L_s} i_{qs} - \frac{\omega_r L_m}{\sigma L_s} i_{dr} + \frac{R_r L_m}{\sigma L_s L_r} i_{qr} + \frac{1}{\sigma L_s} v_{qs} - \frac{L_m}{\sigma L_s L_r} v_{qr} \\ \frac{di_{dr}}{dt} = \frac{R_s L_m}{\sigma L_s L_r} i_{ds} - \frac{\omega_r L_m}{\sigma L_r} i_{qs} - \frac{R_r}{\sigma L_r} i_{dr} + \left( \omega_s - \frac{\omega_r}{\sigma} \right) i_{qr} - \frac{L_m}{\sigma L_s L_r} v_{ds} + \frac{1}{\sigma L_r} v_{dr} \\ \frac{di_{qr}}{dt} = \frac{\omega_r L_m}{\sigma L_r} i_{ds} + \frac{R_s L_m}{\sigma L_s L_r} i_{qs} - \left( \omega_s - \frac{\omega_r}{\sigma} \right) i_{dr} - \frac{R_r}{\sigma L_r} i_{qr} - \frac{L_m}{\sigma L_s L_r} v_{qs} + \frac{1}{\sigma L_r} v_{qr} \end{cases} \quad (1)$$

The stator and rotor flux equations are given as

$$\begin{cases} \phi_{ds} = L_s i_{ds} + L_m i_{dr} \\ \phi_{qs} = L_s i_{qs} + L_m i_{qr} \\ \phi_{dr} = L_m i_{ds} + L_r i_{dr} \\ \phi_{qr} = L_m i_{qs} + L_r i_{qr} \end{cases} \quad (2)$$

The electromagnetic torque can be expressed with stator fluxes and currents as

$$T_{em} = \frac{3p}{2} (\phi_{ds} i_{qs} - \phi_{qs} i_{ds}) \quad (3)$$

The stator active and reactive powers can be expressed as

$$\begin{cases} P_s = \frac{3}{2} (v_{ds} i_{ds} + v_{qs} i_{qs}) \\ Q_s = \frac{3}{2} (v_{qs} i_{ds} - v_{ds} i_{qs}) \end{cases} \quad (4)$$

The mechanical equation that describes rotor speed dynamics is expressed as

$$J \frac{d\omega_{mec}}{dt} = T_{em} - B\omega_{mec} - T_{mec} \quad (5)$$

The relationship between  $\omega_{mec}$  and  $\omega_r$  is  $\omega_r = pole\ pairs \times \omega_{mec}$ .

The wind power model can be expressed according to the mechanical power captured from the wind, which is described as [43]:

$$P_w = \frac{1}{2} \rho A C_p(\lambda, \beta) v_w^3 \quad (6)$$

To maximize the mechanical power extracted by the wind turbine, the rotor speed reference of DFIG-WT is given based on power-speed curve as

$$\omega_{mec}^* = \lambda_{opt} v_w / D \quad (7)$$

where  $\lambda_{opt}$  is the optimal tip-speed ratio that results in the maximum value of  $C_p(\lambda, \beta)$  and  $D$  is the blade length of the wind turbine.

### B. Active/reactive power decoupling control

The proposed controller works with the control framework shown in Fig.2. The stator voltage oriented (SVO) dq frame is used by aligning the q-axis with the stator voltage vector. The proposed controller requires measurements of d- and q-axis rotor currents and the rotor current references are calculated from the stator active and reactive power references, respectively. The rotor speed command can be obtained based on the optimal power-speed curve, and the reactive power reference is set based on power factor requirement. Finally, the required rotor voltages can be applied to rotor winding via rotor-side converter using SPWM techniques.

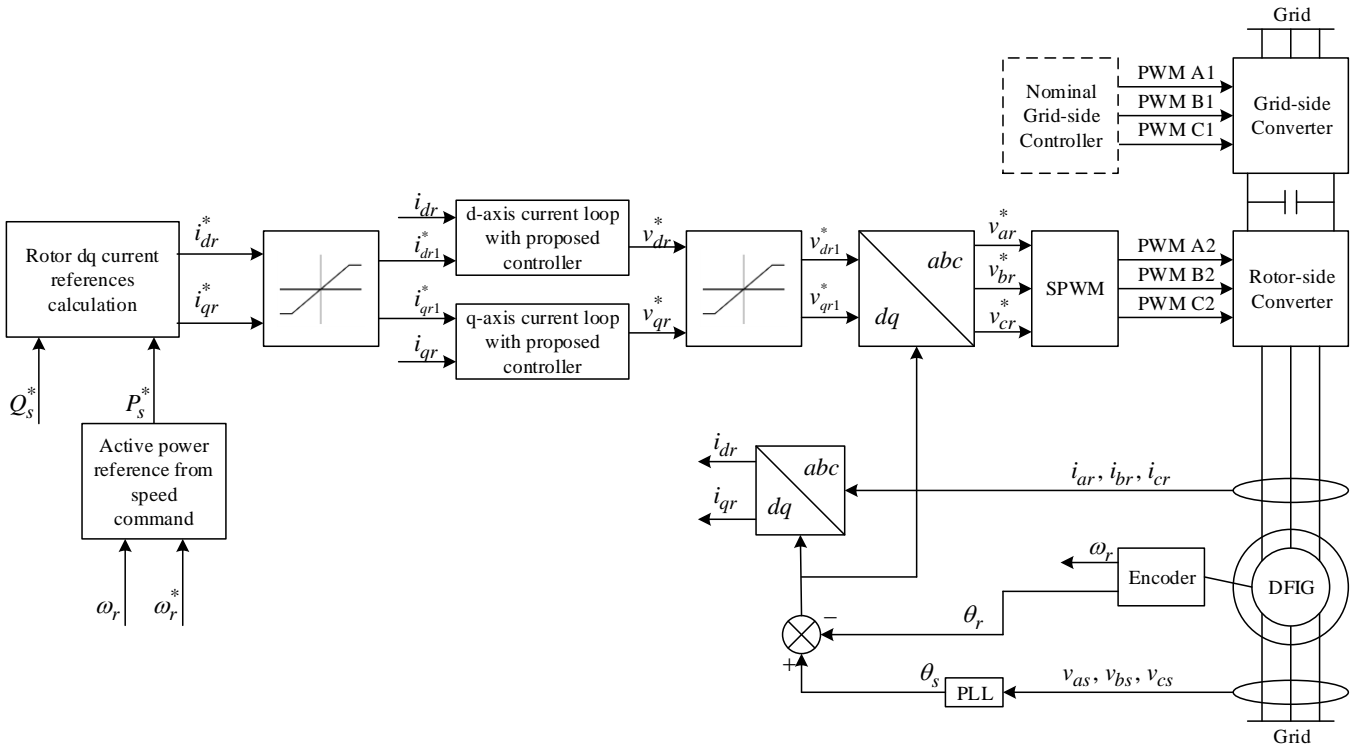


Fig. 2 Control scheme of grid-connected DFIG-WT using proposed controller

For a given active and reactive power references, the d- and q-axis rotor current references can be calculated based on the steady-state relationship between active/reactive power and rotor current as [30]:

$$\begin{cases} i_{dr}^* = \frac{2 L_s Q_s^*}{3 L_m v_{qs}} - \frac{v_{qs}}{\omega_s L_m} \\ i_{qr}^* = \frac{2 L_s P_s^*}{3 L_m v_{qs}} \end{cases} \quad (8)$$

It is noted that the measurement of  $v_{qs}$  in (8) can be replaced by its nominal value, which reduces one measurement input. The active power reference is obtained from the outer speed loop, which converts the speed error into active power reference using PI controller as [44]

$$P_s^* = k_p (\omega_r - \omega_r^*) + k_i \int (\omega_r - \omega_r^*) dt \quad (9)$$

### C. Input-output linearization

The rotor current dynamics in (1) can be rewritten as

$$\begin{cases} \dot{i}_{dr} = f_d + g_d v_{dr} \\ \dot{i}_{qr} = f_q + g_q v_{qr} \end{cases} \quad (10)$$

where

$$\begin{cases} f_d = \frac{R_s L_m}{\sigma L_s L_r} i_{ds} - \frac{\omega_r L_m}{\sigma L_r} i_{qs} - \frac{R_r}{\sigma L_r} i_{dr} + \left( \omega_s - \frac{\omega_r}{\sigma} \right) i_{qr} - \frac{L_m}{\sigma L_s L_r} v_{ds} \\ f_q = \frac{\omega_r L_m}{\sigma L_r} i_{ds} + \frac{R_s L_m}{\sigma L_s L_r} i_{qs} - \left( \omega_s - \frac{\omega_r}{\sigma} \right) i_{dr} - \frac{R_r}{\sigma L_r} i_{qr} - \frac{L_m}{\sigma L_s L_r} v_{qs} \\ g_d = g_q = \frac{1}{\sigma L_r} \end{cases} \quad (11)$$

The rotor current dynamics in (10) can be decoupled and linearized by choosing the control inputs as

$$\begin{cases} v_{dr} = \frac{1}{g_d} (u_d - f_d) \\ v_{qr} = \frac{1}{g_q} (u_q - f_q) \end{cases} \quad (12)$$

which linearizes the system and yields

$$\begin{cases} \dot{i}_{dr} = u_d \\ \dot{i}_{qr} = u_q \end{cases} \quad (13)$$

The feedback control law can be designed for the linear system (13) to achieve the tracking control of

$i_{dr}$ ,  $i_{qr}$  with references  $i_{dr}^*$ ,  $i_{qr}^*$  as

$$\begin{cases} u_d = \dot{i}_{dr}^* - k_d (i_{dr} - i_{dr}^*) \\ u_q = \dot{i}_{qr}^* - k_q (i_{qr} - i_{qr}^*) \end{cases} \quad (14)$$

By substituting (14) into (13), the dynamics of tracking errors  $e_d = i_{dr} - i_{dr}^*$ ,  $e_q = i_{qr} - i_{qr}^*$  can be obtained

as

$$\begin{cases} \dot{e}_d + k_d e_d = 0 \\ \dot{e}_q + k_q e_q = 0 \end{cases} \quad (15)$$

The poles of (15) are placed in the left-half complex plane by choosing positive values for  $k_d$  and  $k_q$  such that the error dynamics are exponentially stable.

#### D. Proposed nonlinear adaptive controller

Perturbation states are defined to include system nonlinearities, cross-couplings between subsystems, parameter uncertainties, and external disturbances. According to (10) and (11), the system perturbation can be expressed as

$$\begin{cases} \Psi_d = f_d + (g_d - g_{d0})v_{dr} \\ \Psi_q = f_q + (g_q - g_{q0})v_{qr} \end{cases} \quad (16)$$

where  $g_{d0}$  and  $g_{q0}$  are the nominal values of  $g_d$  and  $g_q$ , respectively. Then, (10) can be rewritten as

$$\begin{cases} \dot{i}_{dr} = \Psi_d + g_{d0}v_{dr} \\ \dot{i}_{qr} = \Psi_q + g_{q0}v_{qr} \end{cases} \quad (17)$$

The perturbations are treated as the extended-order states, so that new state variables can be defined as  $x_{d1} = i_{dr}$ ,  $x_{d2} = \Psi_d$ ,  $x_{q1} = i_{qr}$ , and  $x_{q2} = \Psi_q$ . By choosing the outputs as  $y_d = x_{d1}$  and  $y_q = x_{q1}$ , (17) can be expressed by two subsystems as

$$\begin{cases} \dot{x}_{d1} = x_{d2} + g_{d0}v_{dr} \\ \dot{x}_{d2} = \dot{\Psi}_d(\bullet) \\ y_d = x_{d1} \end{cases} \quad (18)$$

$$\begin{cases} \dot{x}_{q1} = x_{q2} + g_{q0}v_{qr} \\ \dot{x}_{q2} = \dot{\Psi}_q(\bullet) \\ y_q = x_{q1} \end{cases} \quad (19)$$

Assuming perturbation terms  $\Psi_d$  and  $\Psi_q$  are unknown, the perturbation observer needs to be designed for subsystem (18) and (19) to obtain the estimation of the perturbation states. Here, the linear observer is used in the design of perturbation observers [39]. The perturbation observers for subsystem (18) and (19) are designed as

$$\begin{cases} \dot{\hat{x}}_{d1} = \hat{x}_{d2} + h_{d1}(x_{d1} - \hat{x}_{d1}) + g_{d0}v_{dr} \\ \dot{\hat{x}}_{d2} = h_{d2}(x_{d1} - \hat{x}_{d1}) \end{cases} \quad (20)$$

$$\begin{cases} \dot{\hat{x}}_{q1} = \hat{x}_{q2} + h_{q1}(x_{q1} - \hat{x}_{q1}) + g_{q0}v_{qr} \\ \dot{\hat{x}}_{q2} = h_{q2}(x_{q1} - \hat{x}_{q1}) \end{cases} \quad (21)$$



where  $h_{d1}$ ,  $h_{d2}$  are observer gains of perturbation observer (20) for subsystem (18),  $h_{q1}$ ,  $h_{q2}$  are observer gains of perturbation observer (21) for subsystem (19), and the embellishment ‘ $\hat{\cdot}$ ’ stands for the estimated value of a variable. The pole placement technique is applied for selecting the observer gains such that the observer error dynamics of each subsystem are Hurwitz. The observer gains  $h_{d1}$  and  $h_{d2}$  are selected such that the roots of being in the open left-half plane. Similarly, the observer gains  $h_{q1}$  and  $h_{q2}$  are chosen to place the poles of  $s^2 + h_{q1}s + h_{q2} = 0$  in the open left-half plane.

It should point out that the main contribution of this paper against [28] is that the proposed perturbation observer can estimate unknown fast time-varying unknown dynamics while the observer in [28] can only estimate unknown constant or slow time-varying disturbance based on the assumption of zero change rate of the disturbances. Note that both observers are exponentially convergent with rates by setting correspondent observer gains, but the observer [28] is only valid under the assumption of zero change rate of the disturbances. However, as the converging rate of the observer is usually set to be 5 – 10 times faster than the dynamic of estimated disturbance, the converging rate of the proposed observer will be set much faster than the one in [28], with the cost of a relatively larger observer gains.

Finally, the control inputs can be synthesized based on the linear feedback law (14) and the perturbation observer (20) and (21) as

$$\begin{cases} v_{dr} = \frac{1}{g_{d0}} \left[ \dot{i}_{dr}^* - k_d (i_{dr} - i_{dr}^*) - \hat{\Psi}_d \right] \\ v_{qr} = \frac{1}{g_{q0}} \left[ \dot{i}_{qr}^* - k_q (i_{qr} - i_{qr}^*) - \hat{\Psi}_q \right] \end{cases} \quad (22)$$

As the separation principle of separately designing observer and controller is no longer valid for a nonlinear system, the stability of the overall closed-loop system should be investigated considering all subsystems together, including perturbation observer (20, 21), nonlinear control (22), and the controlled system (1) and (10). The stability analysis of overall closed-loop system is given in **APPENDIX B**.

The block diagram of the proposed controller is shown in Fig.3. The implementation of the proposed controller only requires the information of rotor current states and the nominal value of  $g_{d0}$ ,  $g_{q0}$ . Although the values of the stator currents are not involved in the proposed control loops, the measurement of the stator currents is still needed in the overall control system for DFIG-WT. It implies a simpler structure and less dependency on model information than the FLC. With proper observer gains selected using pole placement techniques, the perturbation observers can actively estimate and compensate perturbations. It is worthy to note that there is a trade-off on observer gain selection between the convergence speed and sensitivity to measurement noise since the increase of observer gains can amplify the measurement noise. **Another contribution of the proposed controller is that the proposed observer (20) – (21) does not rely on the DFIG parameters, which reduces the complexity of the controller and improves**

the robustness to measurement noise and parameter uncertainties as well. This is another contribution of the proposed method comparing to [28].

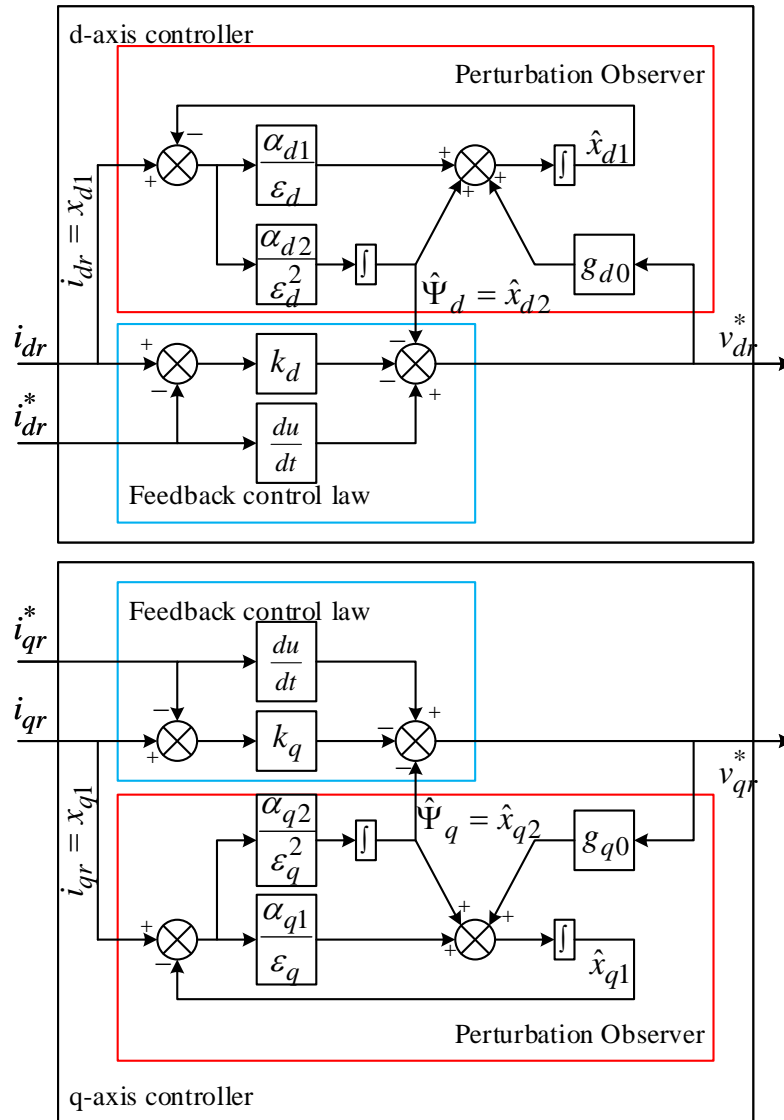


Fig. 3 Control block diagram of proposed controller without saturation of RSC

#### E. Current and voltage saturation strategies for RSC

To consider the voltage and current saturation of the RSC, upper bounds of the voltage and current references need to be set. The priority of the current reference is given to the active power control hence the control of  $i_{qr}^*$  is prioritized [46]. Given  $I_{\max}$  as the upper bound of the current magnitude, the q-axis current reference after saturation is given as

$$i_{qr1}^* = \begin{cases} \text{sign}(i_{qr}^*) \cdot I_{\max}, & |i_{qr}^*| \geq I_{\max} \\ i_{qr}^*, & |i_{qr}^*| < I_{\max} \end{cases} \quad (23)$$

and the d-axis current reference after saturation is

$$i_{dr1}^* = \begin{cases} \text{sign}(i_{dr}^*) \cdot \sqrt{I_{\max}^2 - i_{qr}^{*2}}, & |i_{dr}^*| \geq \sqrt{I_{\max}^2 - i_{qr}^{*2}} \\ i_{dr}^*, & |i_{dr}^*| < \sqrt{I_{\max}^2 - i_{qr}^{*2}} \end{cases} \quad (24)$$

The value of  $I_{\max}$  is set to be the rated value of the rotor current amplitude [47].

With respect to the saturation of the rotor voltage, a general approach in [44] is used, in which the magnitude of the rotor voltage reference, namely  $V_r^* = \sqrt{v_{dr}^{*2} + v_{qr}^{*2}}$ , is limited by setting an upper bound  $V_{\max}$ , which yields

$$V_{r1}^* = \begin{cases} V_{\max}, & V_r^* \geq V_{\max} \\ V_r^*, & V_r^* < V_{\max} \end{cases} \quad (25)$$

while the angle between  $v_{dr}^*$  and  $v_{qr}^*$ , namely  $\theta_r^* = \arctan(v_{qr}^* / v_{dr}^*)$ , is unchanged. Therefore, the rotor voltage references processed by the saturation approach can be obtained by

$$\begin{cases} v_{dr1}^* = V_{r1}^* \cdot \cos \theta_r^* \\ v_{qr1}^* = V_{r1}^* \cdot \sin \theta_r^* \end{cases} \quad (26)$$

With SPWM based VSC control strategy, the amplitude of the maximum achievable fundamental output voltage of VSC without over-modulation is  $V_{dc} / 2$ . As the limit of the dc-link voltage is typically 1.2 times of its nominal value,  $V_{dc\_nom}$ , so  $V_{\max}$  can be set to be  $V_{\max} = 1.2V_{dc\_nom} / 2$ .

### III. SIMULATION STUDIES

The performance of the proposed nonlinear adaptive controller (NAC) has been tested via simulation in Matlab/Simulink. The simulated system is based on the demo with the detailed model of a DFIG-WT and power converters provided by the SimPowerSystems library. Comparison studies have been undertaken among the conventional vector control (VC), the disturbance observer based feedback linearizing control (DOFLC) proposed in [28], and the proposed NAC. The DOFLC has been briefly recalled in Appendix A. The controllers designed in the continuous-time domain have been discretized using forward Euler's method for digital control implementation. The PWM frequency is set as 5 kHz with SPWM technique.

When implementing the perturbation observer in simulation, the observer gains are selected as  $h_{d1} = h_{q1} = 2 \times 10^4$  and  $h_{d2} = h_{q2} = 1 \times 10^8$  so all poles of the observer error dynamics are placed at  $\gamma = 10000$ . The values of  $g_{d0}$  and  $g_{q0}$  are constants obtained based on the system parameters.

**Table I Parameters of the simulated DFIG-WT**

Nominal power	1.5/0.9 MVA	Nominal voltage	575 Vrms 60 Hz
Pole pairs	3	Stator/rotor turns ratio	1:3
Stator resistance	0.0026 $\Omega$ (0.023 pu)	Rotor resistance	0.0029 $\Omega$ (0.016 pu)
Stator leakage inductance	0.077 mH (0.18 pu)	Rotor leakage inductance	0.083 mH (0.16 pu)

Mutual inductance	2.5 mH (2.9 pu)	Inertia constant	0.685 s
Wind speed	12 m/s	Initial rotor speed	1.2 pu
Transmission Line length	10 km	No. of wind turbines	1

#### A. Decoupled control of active/reactive power under step references

The decoupled control of the active and reactive power of the DFIG is tested by evaluating the step responses of the active and the reactive power. The step functions of references are filtered by a transfer function such that the fast change of reference values can be avoided. The simulation results are shown in Fig. 5, which indicates that the DOFLC and the NAC provide the faster speed of response than the VC does. The NAC has the same step change performance as the DOFLC. With no uncertainty and all external disturbance correctly measured, the DOFLC provide the same performance as FLC as the disturbance observer in DOFLC doesn't make an effort to estimate the uncertainty. So, the simulation result suggests that the proposed NAC is able to provide the dynamic performance as good as the FLC does.

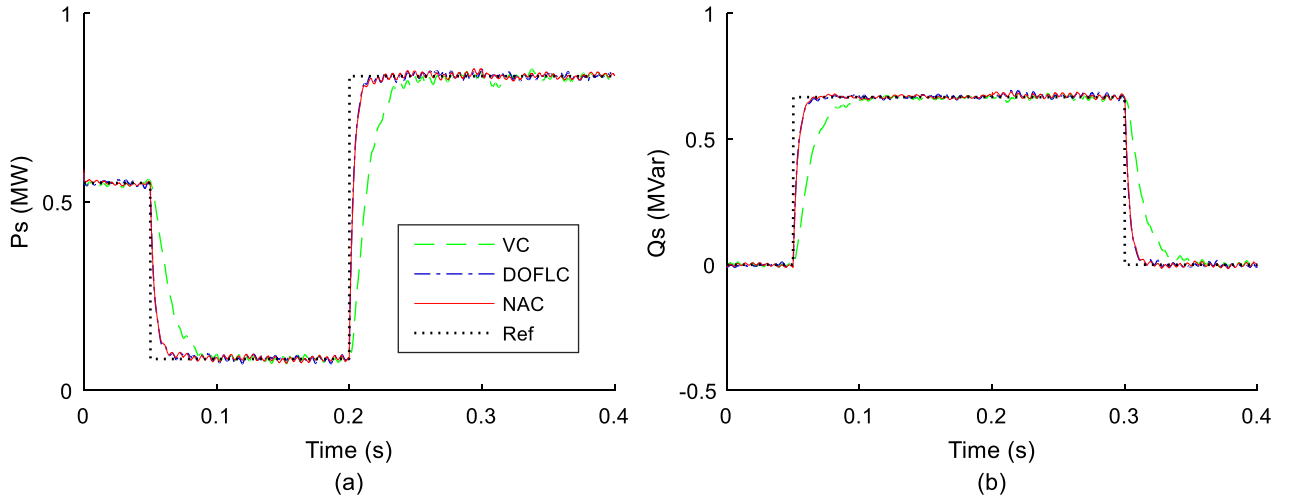


**Fig.4 Step responses of the stator power: (a) active power, (b) reactive power.**

#### B. Decoupled control of active/reactive power under sinusoidal references and uncertainties

The DFIG may be required to generate sinusoidal active/reactive power in case of the demand for system damping [28]. The tracking performance of sinusoidal reference has been tested. Moreover, uncertainties including a time-varying unknown rotor resistance and a 20% mismatched error of  $L_m$  in the controllers have been introduced. Fig. 5 shows the time-varying rotor resistance applied in the simulation. The tracking performance of the sinusoidal reference is shown in Fig. 6. There is a 20 Hz sinusoidal signal with 0.6 MW amplitude added to the active power reference at  $t = 0.1 s$  and then a 20 Hz sinusoidal signal with 0.6 MVar amplitude is added to the reactive power reference at  $t = 0.2 s$ . The tracking performance provided by the VC has an obvious lag between the power references and the real active/reactive power. The tracking errors are shown in Fig. 7, in which the NAC is with the maximum

tracking error of 0.1 MW and 0.05 MVar, the VC is with maximum tracking errors of 0.43 MW and 0.48 MVar while the DOFLC is with 0.2 MW and 0.24 MVar maximum tracking errors. The fast time-varying uncertainties in the tracking control caused by the time-varying rotor resistance and the mismatch value of inductance can be actively estimated and compensated by the estimated perturbations using the perturbation observer of the NAC. The tracking performance with fast time-varying uncertainty is improved when using the proposed NAC.

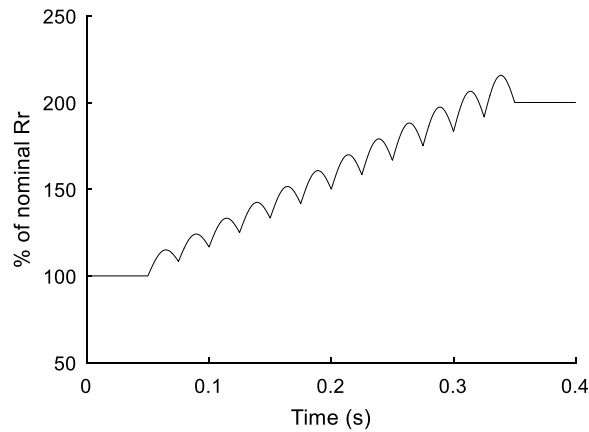


**Fig.5 Actual value of rotor resistance**

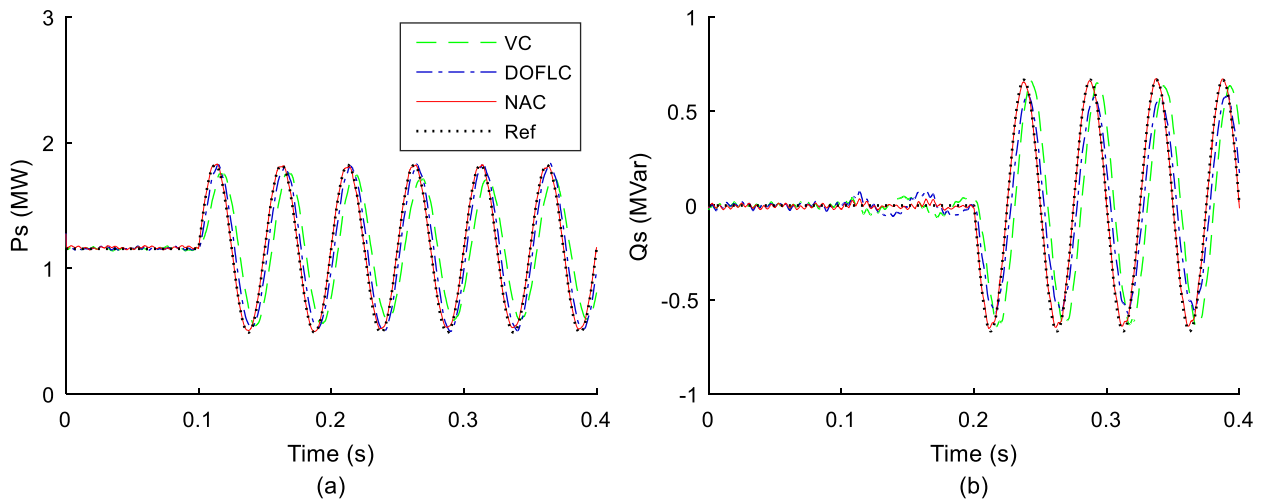


**Fig.6 Power reference tracking with uncertainties: (a) active power, (b) reactive power.**

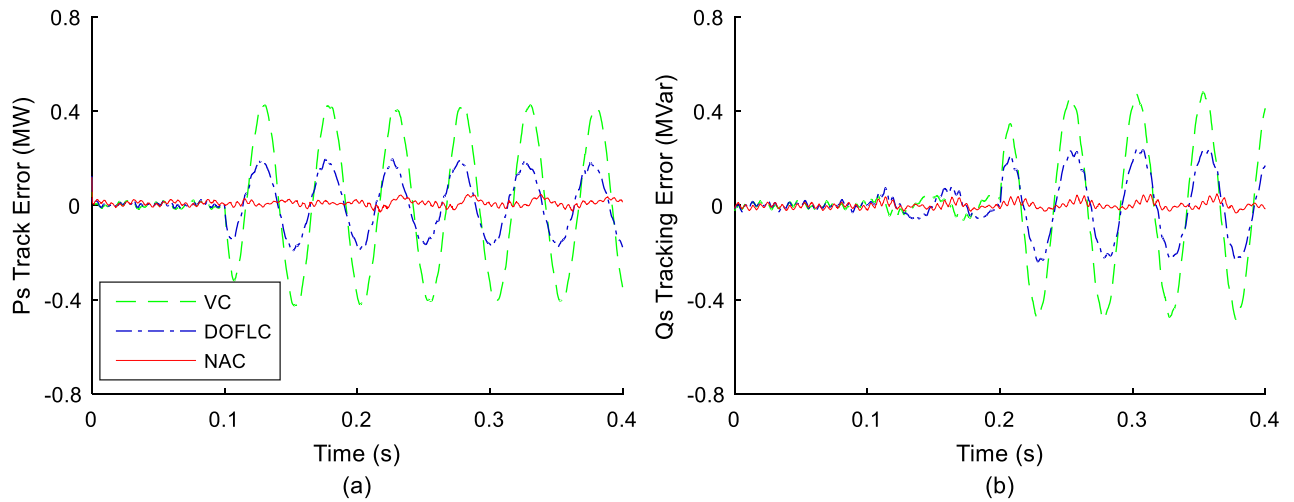


**Fig.7 Tracking errors with uncertainties: (a) active power, (b) reactive power.**

### C. Low-voltage ride-through (LVRT) capabilities with uncertainty

The voltage dip happened at the stator terminal will cause large inrush current that may damage the power electronic devices and trip the wind energy system. The LVRT capabilities of the DFIG with three controllers have been evaluated via examining the rotor current response to the voltage dip. The 20% mismatched error of the value of  $L_m$  is applied in controllers during simulation. It is shown in Fig. 8(a) that a 20% dip of grid voltage is applied at  $t = 0.05\text{ s} - 0.15\text{ s}$  while the DFIG-WT is operating at steady state with 1.2 pu rotor speed. Fig.8(b) shows the rotor current magnitude in response to this voltage dip. The peak transient current of the DFIG with the VC is 1.05 kA, whereas the peak rotor current with DOFLC and NAC is 0.72 kA and 0.68 kA, respectively. With NAC, the peak rotor current during and after the voltage dip is reduced by 35% compared to VC and 5% comparing to DOFLC. The NAC also reduces the oscillations of the rotor current amplitude and recover to its pre-fault value fast after the restoration of the grid voltage. With mismatched mutual inductance, the disturbance and perturbation observers need to estimate fast time-varying disturbances during the voltage dip due to the oscillating of the natural flux. Therefore the advantage of estimating fast time-varying with proposed perturbation observers is revealed.

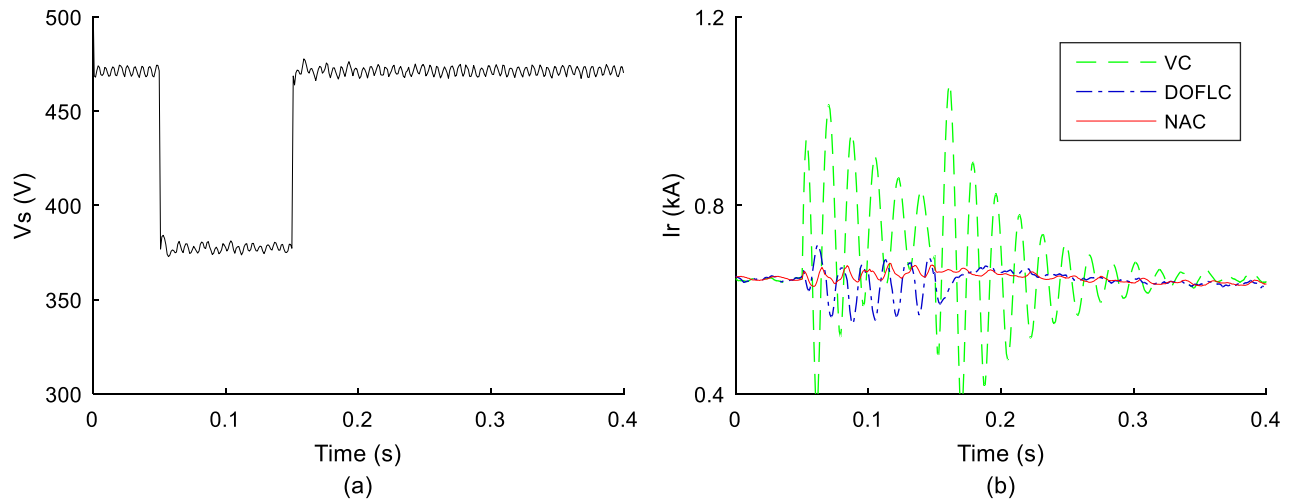


**Fig.8 Responses of rotor current magnitude to the 20% dip of stator terminal voltages with uncertainty: (a) stator voltage magnitude, (b) rotor current magnitude**

The RSC controller will increase the rotor voltage to compensate the disturbance caused by the voltage dip at the stator and so as to constrain the converter current. To demonstrate the effect of the saturation of RSC, the rotor voltage amplitude from three controllers are shown in Fig. 9, in which rotor voltage from all cases has been limited below the  $V_{max}$ . Note that 20% voltage dip is used in this case, it can predict that under a case with a bigger voltage dip level, the amplitude of the rotor voltage will increase and approach more closely to the  $V_{max}$ .

The rotor current is jointly decided by the injected rotor voltage via RSC and the induced electromotive force (EMF) [49]. During the transient period under the voltage dip, the induced EMF is consequently large. To compensate the induced EMF, a large output voltage of RSC is expected to reduce the rotor current. The result shows that both the DOFLC and the proposed NAC require larger output voltage of the RSC to constrain the transient rotor current when comparing to the VC. And the NAC requires a smaller rotor voltage than the DOFLC and results in a smaller rotor current. Note that for both NAC and DOFLC, the induced EMF component is same under the same voltage dip level. However, the DOFLC cannot accurately estimate the disturbance under the voltage dip in the presence of the mismatched parameter  $L_m$  as the disturbance changes quickly, which results in the induced transient components cannot be completely compensated. As both NAC and DOFLC use the same linear controller, the inaccurate compensation with DOFLC causes a larger peak rotor current and longer oscillation period whereas the NAC can accurately estimate the disturbance hence a smaller peak value and shorter oscillation period.

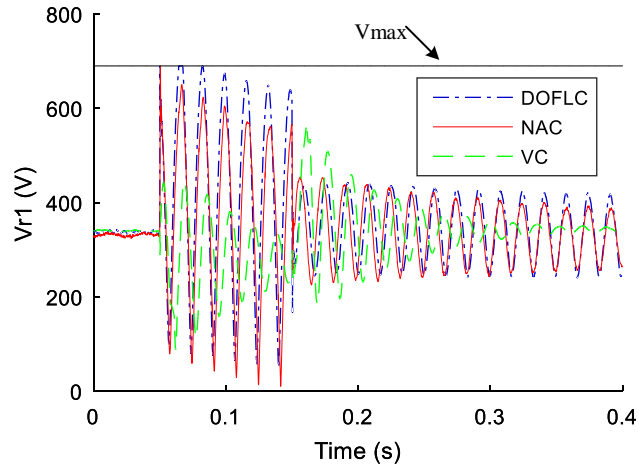


**Fig.9 Amplitude of the calculated rotor voltage after saturation during and after a voltage dip**

#### *D. Robustness against measurement noise*

Sensor noise is inevitable and will degrade the control performance by distorting the controlled system inputs. To test the controller performance with measurement noise, a Gaussian noise with 0 mean and variance 2% of the signals' true RMS values is applied. The maximum value of the noise is limited to 5% of the true RMS values. The active/reactive power performance and stator current THD in steady state are studied in Fig. 10 and Fig. 11, respectively. The DFIG with DOFLC has more serious distortion in both active and reactive power, while the influence of noise in NAC is smaller with NAC. With respect to the THD performance shown in Fig.10, the DOFLC results in a higher stator current THD (peak value is 2.7%) than NAC (peak value is 0.7%). Although the observers magnify the noise and cause distortion in controlled variables, which is the drawback of both DOFLC and NAC, the proposed NAC does not need full state feedbacks so the noise of stator voltages and currents can be isolated with NAC.

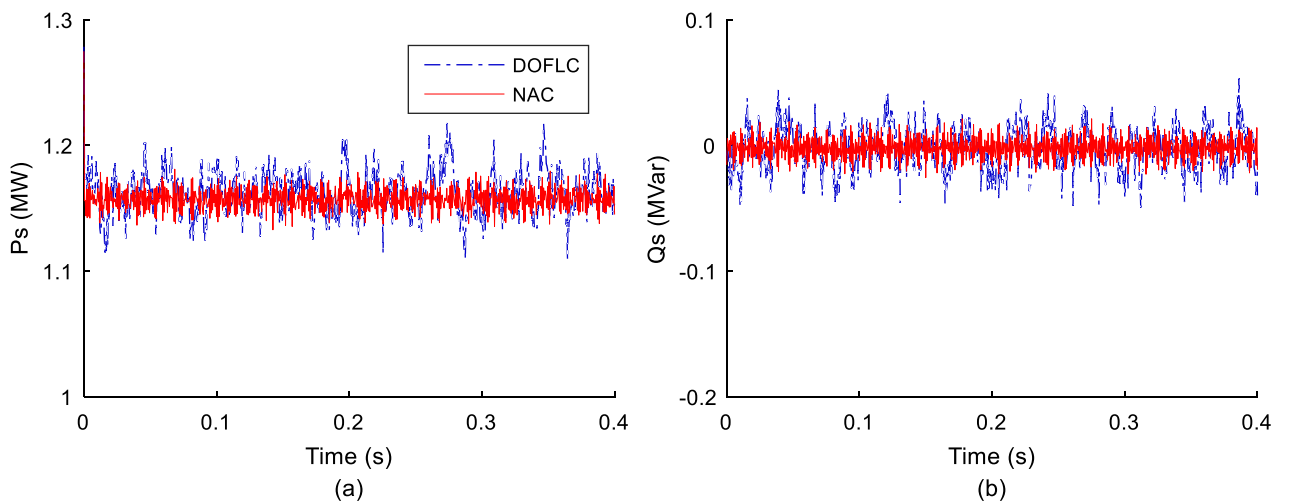


**Fig.10 Steady-state performance of DFIG with measurement noise: (a) stator active power, (b) stator reactive power.**



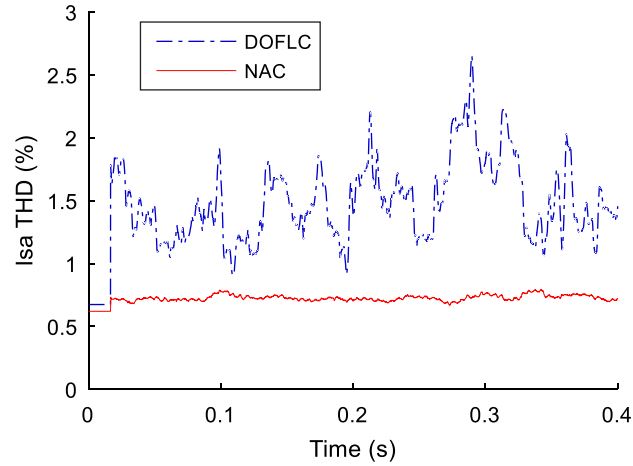


**Fig.11 The THD of phase A stator current with measurement noise.**

#### IV. EXPERIMENTAL VALIDATION

Fig. 12 shows the experimental setup of the DFIG system with back-to-back IGBT converters. A 2kW DFIG (LabVolt 8505-A0) is driven by an AC motor (LabVolt 8540), the rotor windings of DFIG are connected to two back-to-back IGBT converters (LabVolt 8857-10), and the stator windings are supplied by a 110 V 50 Hz three-phase voltage via a Variac that is connected to a 240 V 50 Hz three-phase socket. The controllers are implemented using OP4500 simulator with analog signals from the voltage/current measurement units, and digital signals from an encoder fed in. The converters are driven by duty-cycle controlled PWM signals, which are generated by OP4500 simulator. The experiment system parameters are listed in Table III.

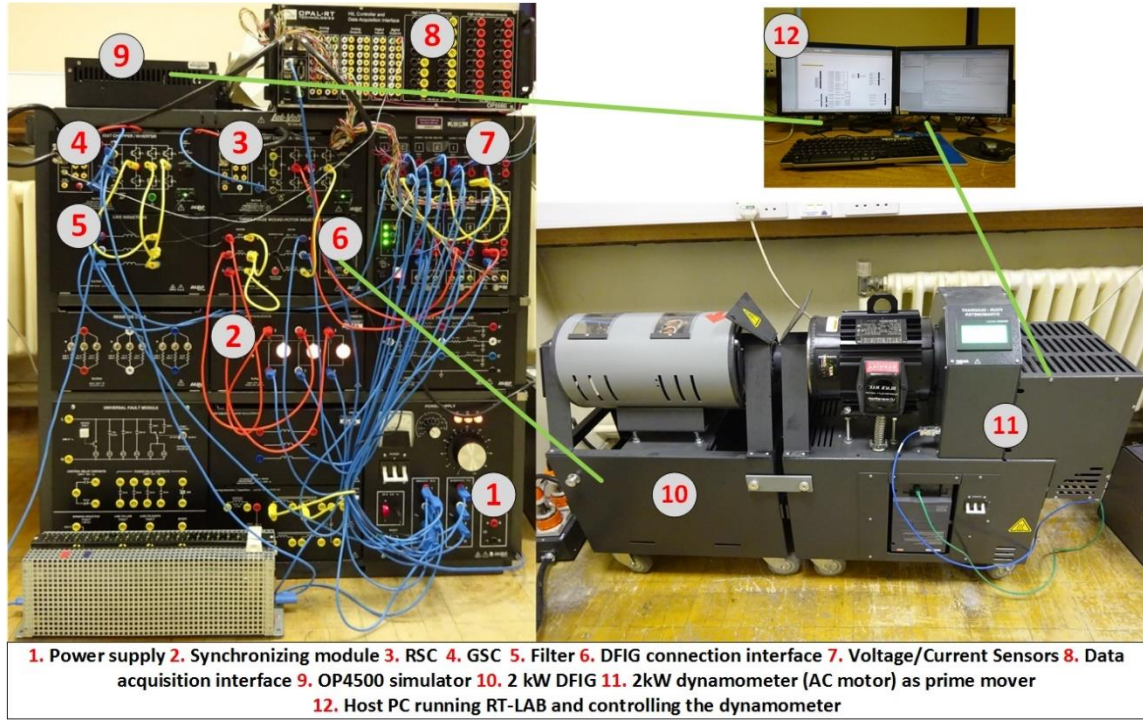


**Fig.12 Experimental setup with LabVolt 2kW DFIG kit and OP4500 simulator**

**Table III Parameters of LabVolt 2kW DFIG System**

Rated power	2 kW	Stator voltage	110 V 50Hz
Pole pairs	2	Stator/rotor turns ratio	0.3
Stator resistance	2.3 $\Omega$	Rotor resistance	2.5 $\Omega$
Stator leakage inductance	0.02 H	Rotor leakage inductance	0.02 H
Mutual inductance	0.35 H	Inertia constant	0.107 kg.m <sup>2</sup>
Filter inductance	0.06 H	DC voltage	400 V
PWM frequency	5000 Hz		

#### A. Decoupled control of active and reactive power outputs

The decoupled active/reactive power control with the proposed controller is tested at 1800 RPM (1.2 pu) rotor speed, which is shown in Fig. 12. The step changes between 1 kW and 0.5 kW are applied to active power, and step changes between 0 Var and 500 Var are applied to reactive power. Fig. 12(a) shows the decrease of active power while reactive power keeps constant, whereas Fig. 12(b) shows the step up of reactive power while active power is constant. Fig. 12(c) and Fig. 12(d) present the simultaneous change of active and reactive power. The control of active/reactive power with NAC can be fully decoupled, and the step response is fast (within 20 ms) without overshoots and oscillations.

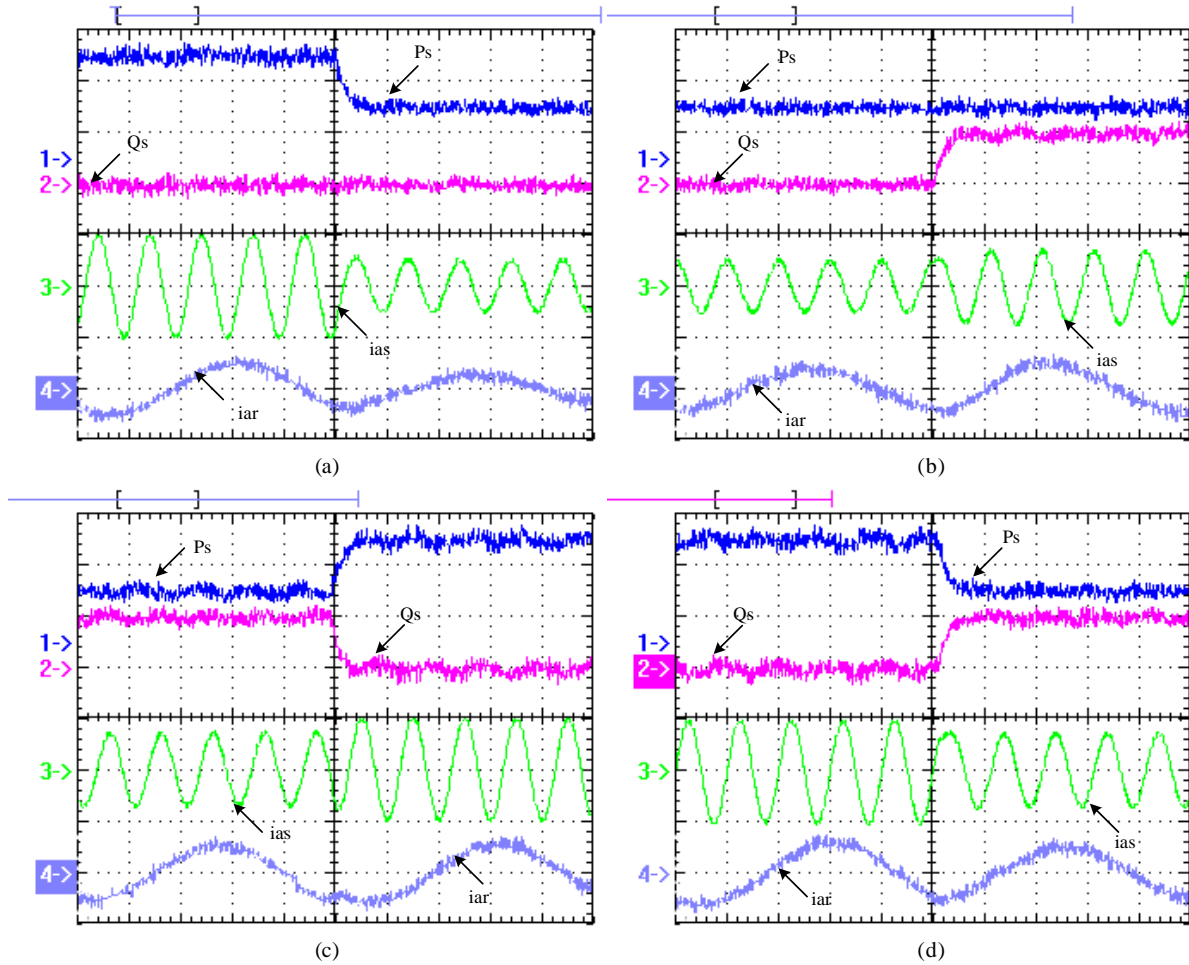


**Fig.13 The DFIG active/reactive power step response with NAC: (a) step down of  $P_s$ , (b) step up of  $Q_s$ , (c) step up of  $P_s$  and step down of  $Q_s$ , (d) step down of  $P_s$  and step up of  $Q_s$  (Divisions:  $P_s - 500$  W/div,  $Q_s - 500$  Var/div,  $i_{as} - 6$  A/div,  $i_{ar} - 2$  A/div, time - 20 ms/div).**

### B. Operation at different operating points

Further tests of the active/reactive power control at different rotor speed have been done, and the experiment results are shown in Fig. 13. It can be observed that the step response of VC is slower than DOFLC NAC and has small overshoots in Fig. 13 (a) and 13 (b) when the DFIG operates at the super-synchronous speed. In comparison, Fig. 13 (c) and 13 (d) show the step response at sub-synchronous rotating speed. The larger overshoot and more oscillations can be observed with VC when comparing to the VC responses at super-synchronous. The varying of operation points can cause the performance degradation when using VC, whereas it does not impact the performance of DOFLC and NAC.

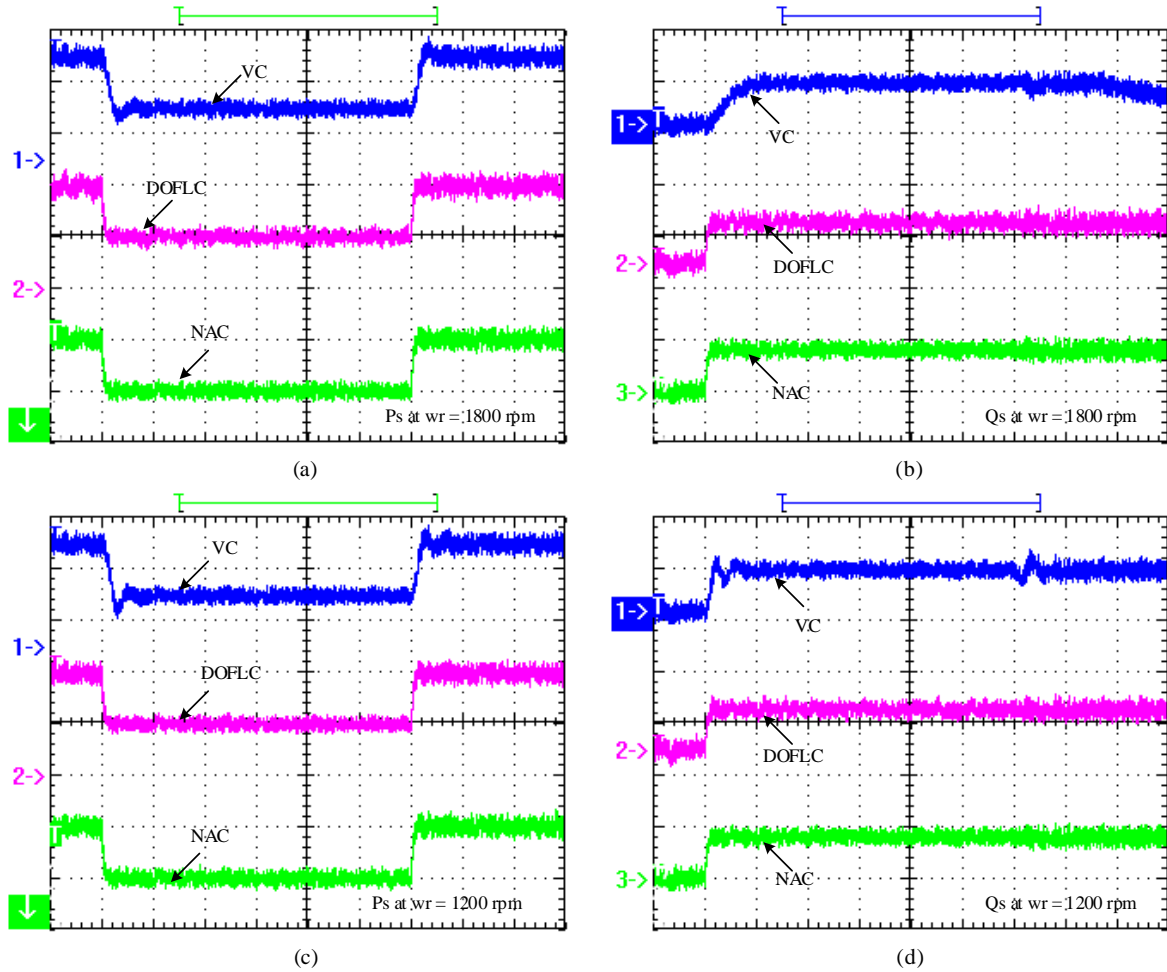


**Fig.14 The DFIG active/reactive power step response at different rotor speeds: (a) Ps at  $w_r=1800$  rpm (b) Qs at  $w_r=1800$  rpm, (c) Ps at  $w_r = 1200$  rpm, (d) Qs at  $w_r = 1200$  rpm (Divisions: Ps – 500 W/div, Qs – 500 Var/div, time-100 ms/div).**

### C. Robustness against parameter uncertainties

In order to emulate the parameter variations, variable resistors are connected in series between converter and rotor windings. A sudden change of the variable resistors from  $0 \Omega$  to  $5 \Omega$  is applied when the DFIG is operating at steady state. And a 20% mismatched error of the value of  $L_m$  is applied. The experiment results are shown in Fig.14(a) and (b). Fig. 14(a) shows that the DFIG controlled by VC has a 400W drop of active power, which is recovered to the set point in 40 ms. With DOFLC, the influence of the fast change of rotor resistance is reduced and a 150W drop of the active power is observed. With proposed NAC, there is no significant influence of rotor resistance variation shown on the active/reactive power due to the ability of NAC in estimating fast-varying uncertainties.

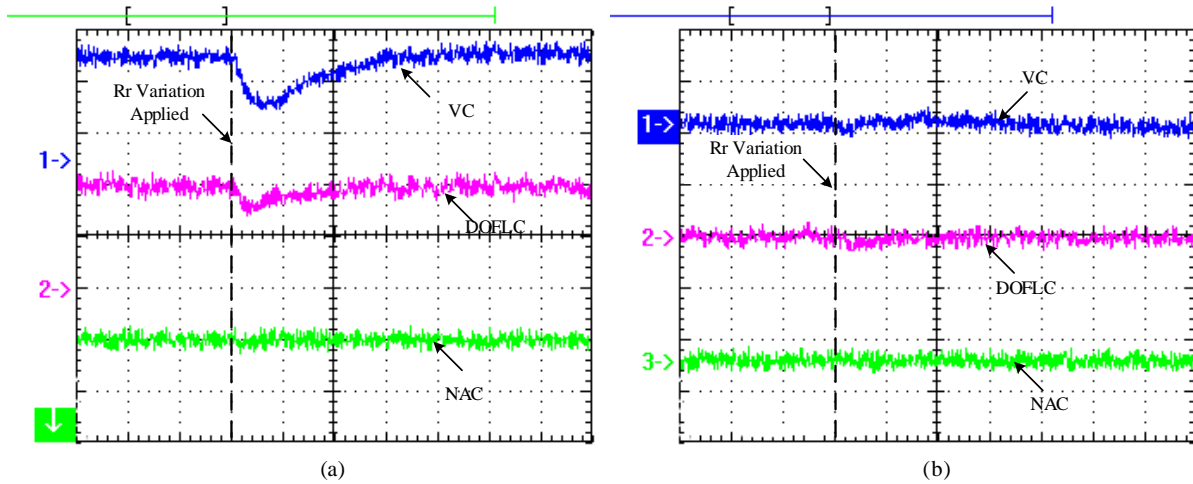


**Fig.15 The DFIG active/reactive power response with uncertainty: (a) active power (b) reactive power (Divisions:  $P_s$  – 500 W/div,  $Q_s$  – 500 Var/div, time-20 ms/div).**

#### D. Sinusoidal power reference tracking with parameter uncertainties

The sinusoidal power reference tracking control has been tested, and the experiment results are shown in Fig. 16. A 20 Hz sinusoidal active and reactive power references are applied in addition to constant power references, which are 500W for active power reference and 0Var for reactive power reference. The amplitudes of the sinusoidal active and reactive power references are 300W and 300Var, respectively. A 20% mismatched error of the value of  $L_m$  is applied. When the active power and the reactive power are controlled to track sinusoidal references, the stator and rotor currents are neither balanced under the balanced grid conditions nor in sinusoidal shapes. The comparison results of the tracking control performance are presented in Fig. 17. With VC, the maximum tracking errors of the active and the reactive power are around 500W and 500Var, respectively. The DFIG controlled by the DOFLC or the NAC results in relatively smaller tracking errors, whose maximum values are less than 300W for active power and 300 Var for reactive power. Comparing Fig. 17 with the simulation results in Fig. 7, the tracking errors with NAC in Fig. 17 can be seen easily due to the higher control time-delay and the smaller observer gains in experimental tests than simulation studies. However, Fig. 17 still suggests the smaller tracking error with NAC than with DOFLC, which draws the same conclusion as the simulation studies.

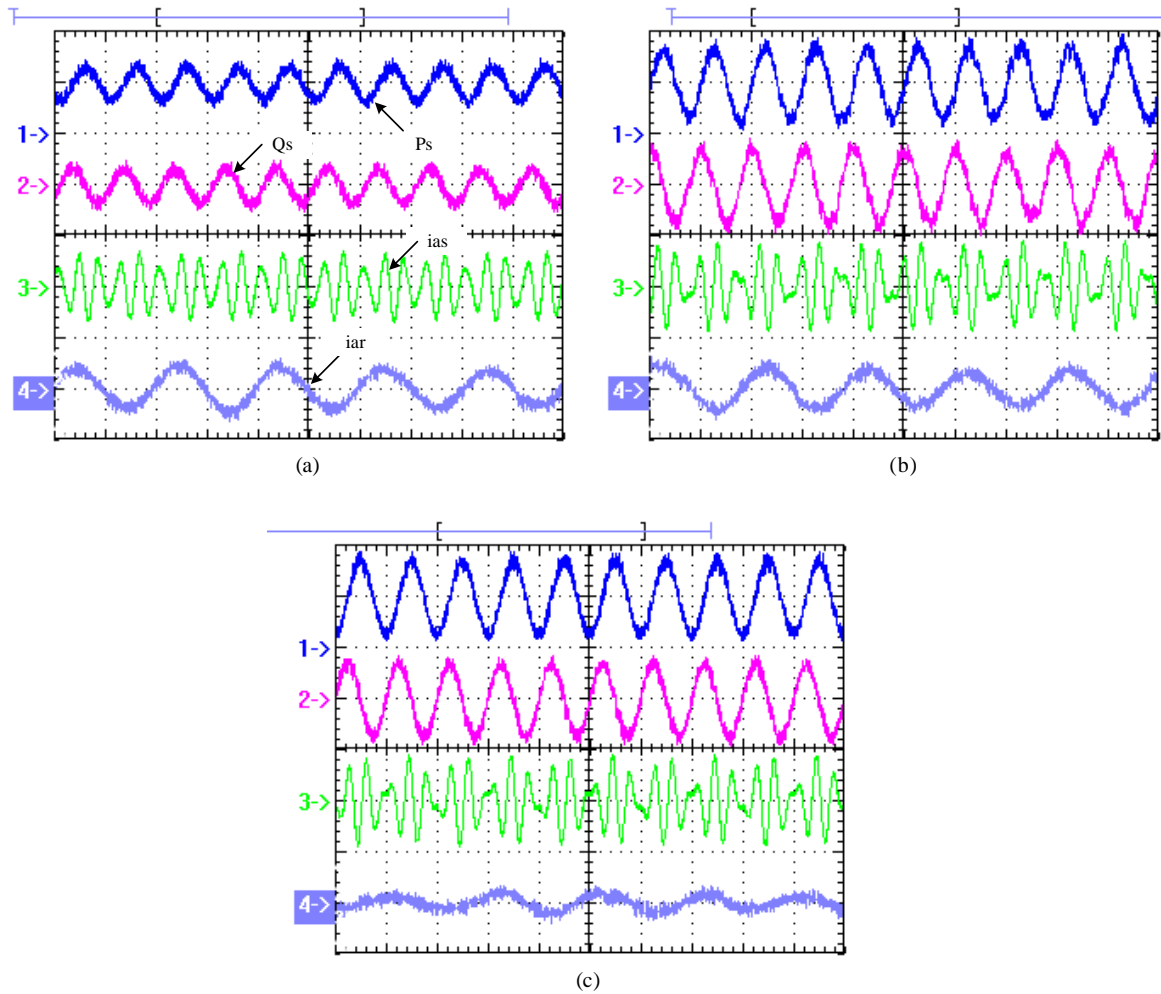


**Fig.16 The DFIG active/reactive power tracking control responses with sinusoidal references applied and uncertainty: (a) VC, (b) DOFLC, (c) NAC (Divisions:  $P_s$  – 500 W/div,  $Q_s$  – 500 Var/div, time-50 ms/div).**

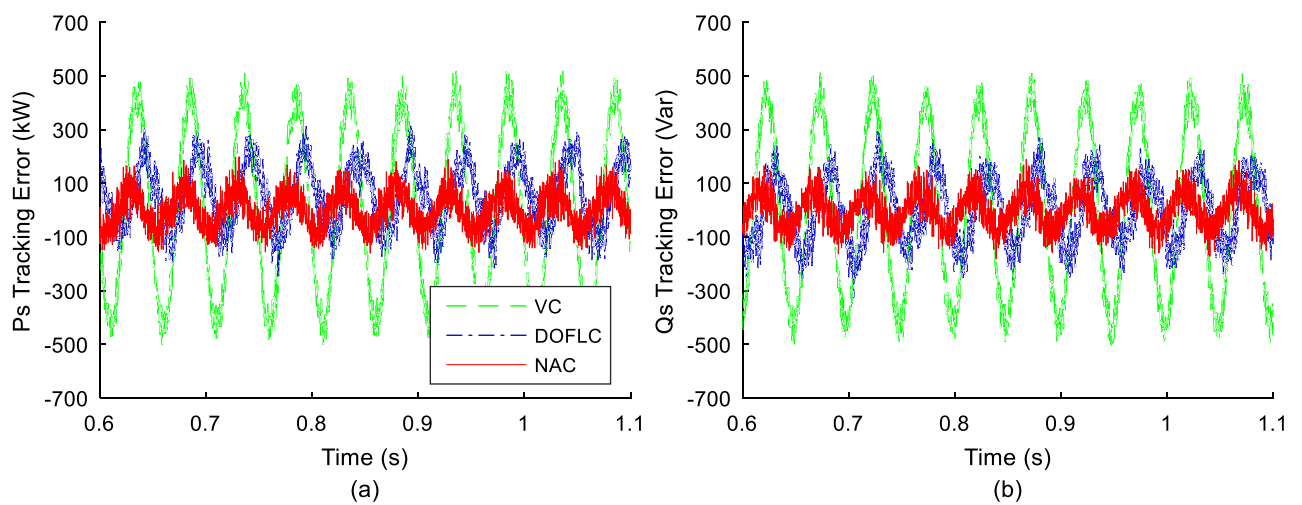


**Fig.17 Tracking errors with sinusoidal reference with uncertainties: (a) active power, (b) reactive power.**

E. LVRT capability considering parameter uncertainties

A 20% dip (30 V) of the stator voltage is applied via turning the Variac with a 20% mismatched error of  $L_m$  to test the DFIG responses to voltage dips. The responses of DFIG controlled by VC, DOFLC, and NAC are shown in Fig.15. It can be observed in Fig. 15(a) that there are oscillations of active/reactive power with VC and the increase of stator current when the voltage dip is applied. The small increase and distortion can also be observed in the rotor current of the DFIG controlled by VC at the same time. In comparison, no significant oscillation of power or inrush current can be observed in Fig.15(b) and Fig.15(c) with DOFLC or NAC. The THD values of the stator current with those controllers are shown in Fig.15(d), which presents in detail of the impacts of the voltage dip in stator current. It's significant that the use of VC results in large distortion of stator current when voltage dip is applied. There is around 2% increase of the THD by using DOFLC when voltage dips. With NAC, the voltage dip causes the smallest distortion of stator current when comparing to the VC and DOFLC. The comparison result verifies that the NAC improves the LVRT capability with uncertainty.

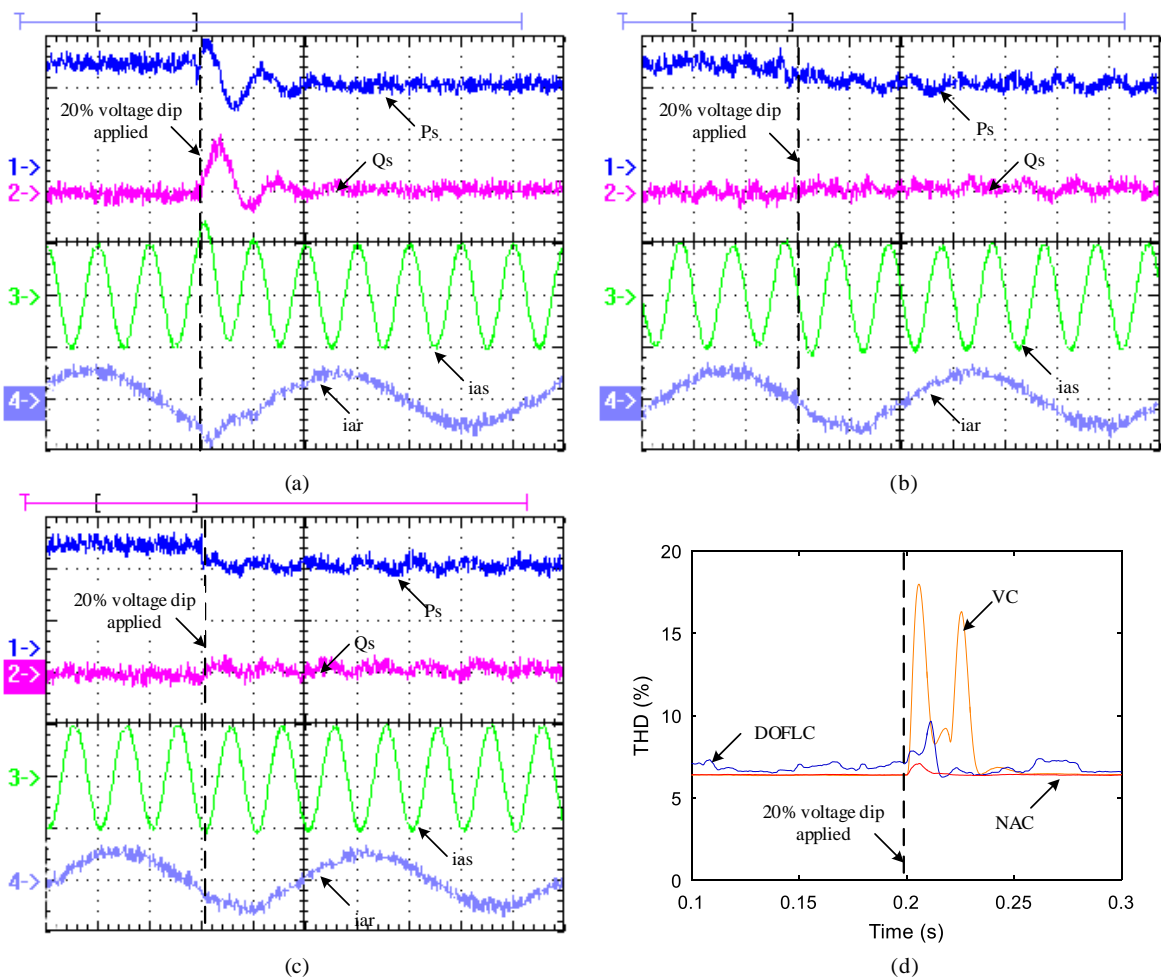


**Fig.18 The LVRT capability test with uncertainty: (a) VC, (b) DOFLC, (c) NAC, (d) stator current THD comparison of three controllers. (Divisions:  $P_s$  – 500W/div,  $Q_s$  – 500 Var/div,  $i_{as}$  – 6 A/div,  $i_{ar}$  – 2 A/div, time-20 ms/div)**

In Fig. 19, the amplitude of calculated rotor voltage after saturation is depicted. The outputs of those controllers in comparative studies do not exceed the maximum amplitude of the RSC when a 20% voltage dip is applied. The DOFLC and the NAC generate a higher oscillated amplitude of the rotor voltage than the VC in order to compensate the disturbance caused by the voltage dip. With fast time-varying disturbance, the DOFLC cannot accurately estimate the actual disturbance, which results in larger rotor voltage and worse transient performance of the current dynamic than the NAC, as shown in Fig. 18(d).

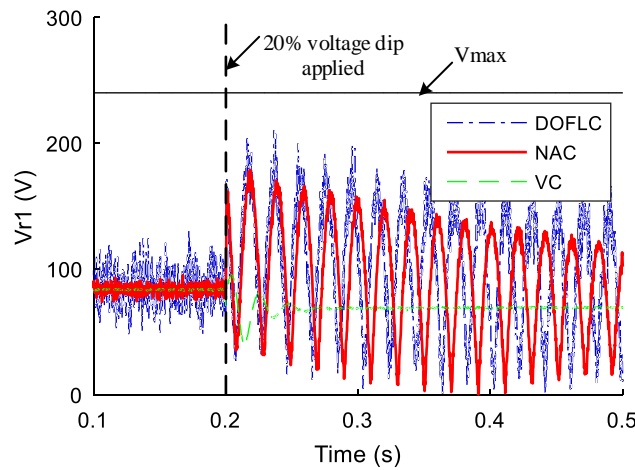


**Fig.19 Experiment result of the amplitude of calculated rotor voltage after saturation during a voltage dip**

## V. CONCLUSIONS

A perturbation estimation based NAC has been proposed for decoupled control of the active/reactive power of the DFIG. The simulation and experiment tests have suggested that the proposed NAC provides fast dynamic response, strong robustness against parameter uncertainties, and improved LVRT capacities even with uncertainties. The perturbation observer is featured of estimating fast time-varying perturbations. Thus the proposed NAC is capable of maintaining good dynamic performance when there are fast variations or mismatched values of system parameters during the transient processes of power tracking control or voltage dip responses. Moreover, the proposed NAC does not require full-state feedback and the detailed system model information, which implies that it has a simpler control structure than other nonlinear controllers. The measurement noises of the stator currents and voltages do not affect the performance of the proposed NAC.



## APPENDIX A

### Disturbance observer based FLC [28]

The DOFLC proposed in [28] is recalled here. A generic parameter  $P$  is defined as  $P \in \{R_r, R_s, L_m, L_s, L_r, \sigma\}$  that includes all possible parameters of DFIG. The actual value of  $P$  can be presented by its nominal value plus uncertainty as  $P = P_0 + \Delta P$ . Then, the rotor current dynamics described in (10) can be rewritten as

$$\begin{cases} \dot{i}_{dr} = f_{d0} + g_{d0}v_{dr} + \Delta_d \\ \dot{i}_{qr} = f_{q0} + g_{q0}v_{qr} + \Delta_q \end{cases} \quad (A1)$$

where  $f_{d0}$ ,  $f_{q0}$ ,  $g_{d0}$ , and  $g_{q0}$  are the values of  $f_d$ ,  $f_q$ ,  $g_d$ , and  $g_q$  with nominal system parameters.

$\Delta_{d,q}$  is defined to include all uncertainties, namely  $\Delta_{d,q} = \Delta_{d,q}(\Delta P, i_{dr}, i_{qr}, i_{ds}, i_{qs}, v_{dr}, v_{qr}, v_{ds}, v_{qs})$ .

A reduced-order observer is designed to estimate the disturbance terms  $\Delta_d$  and  $\Delta_q$ , the estimated terms are denoted as  $\hat{\Delta}_d$  and  $\hat{\Delta}_q$ . The final DOFLC strategy for rotor current control can be expressed as

$$\begin{cases} v_{dr}^* = \frac{1}{g_{d0}} \left[ i_{dr}^* - k_d (i_{dr} - i_{dr}^*) - f_{d0} - \hat{\Delta}_d \right] \\ v_{qr}^* = \frac{1}{g_{q0}} \left[ i_{qr}^* - k_q (i_{qr} - i_{qr}^*) - f_{q0} - \hat{\Delta}_q \right] \end{cases} \quad (A2)$$

In simulation studies of this paper, the observer gains of DOFLC is chosen to be  $G_p = 2000$ .

## APPENDIX B

### Stability analysis of closed-loop system

The stability of the closed-loop system including controller/observer are investigated in this appendix, based on the approach in [39, 48]. For the convenient of stability analysis, observers (20) - (21) have been represented in a compact form as

$$\begin{cases} \dot{\hat{x}}_{i1} = \hat{x}_{i2} + h_{i1}(x_{i1} - \hat{x}_{i1}) + b_{i0}u_i \\ \dot{\hat{x}}_{i2} = h_{i2}(x_{i1} - \hat{x}_{i1}) \end{cases} \quad (B1)$$

where  $\tilde{x}_{ij} = x_{ij} - \hat{x}_{ij}$  refers to the estimation error of  $x_{ij}$ ,  $i=d, q$ ,  $j=1, 2$ .

By choosing

$$h_{i1} = \frac{\alpha_{i1}}{\varepsilon_i} \quad h_{i2} = \frac{\alpha_{i2}}{\varepsilon_i^2} \quad (B2)$$

and defining the scaled estimation errors

$$\eta_{i1} = \frac{\tilde{x}_{i1}}{\varepsilon_i} \quad \eta_{i2} = \tilde{x}_{i2} \quad (B3)$$

the observer error equation can be represented as

$$\varepsilon_i \dot{\eta}_{p_{o_i}} = A_{p_{o_i}} \eta_{p_{o_i}} + \varepsilon_i B_{p_{o_i}} \dot{\psi}_i \quad (\text{B4})$$

where  $\eta_{p_{o_i}} = [\eta_{i1} \eta_{i2}]^T$

$$A_{p_{o_i}} = \begin{bmatrix} -\alpha_{i1} & 1 \\ -\alpha_{i2} & 0 \end{bmatrix} \quad B_{p_{o_i}} = \begin{bmatrix} 0 \\ 1 \end{bmatrix} \quad (\text{B5})$$

The positive constants  $\alpha_{i1}$  and  $\alpha_{i2}$  are chosen such that  $A_{p_{o_i}}$  is a Hurwitzian matrix, and  $\varepsilon_i$ ,  $0 < \varepsilon_i \ll 1$ , is a small positive parameter to be specified. This equation shows clearly that reducing  $\varepsilon_i$  diminishes the effect of the  $\dot{\psi}_i$ . It also shows that, for  $\varepsilon_i$  small enough, the dynamics of the estimation error will be much faster than that of  $x_i$ .

Substituting control (22) into system (17), we have

$$\begin{cases} \dot{i}_{dr} = i_{dr}^* - k_d (i_{dr} - i_{dr}^*) + \tilde{\Psi}_d \\ \dot{i}_{qr} = i_{qr}^* - k_q (i_{qr} - i_{qr}^*) + \tilde{\Psi}_q \end{cases}$$

and defining tracking errors as  $e_d = i_{dr} - i_{dr}^*$  and  $e_q = i_{qr} - i_{qr}^*$ , thus the dynamic of tracking errors is

$$\begin{cases} \dot{e}_d = -k_d e_d + \eta_{d2} \\ \dot{e}_q = -k_q e_q + \eta_{q2} \end{cases}$$

then

$$\dot{e}_i = A_{i0} e_i + B_{i0} \eta_{i2}$$

where  $i = d, q$ ,  $A_{i0} = [-k_i]$ , and  $B_{i0} = [1]$ .

The closed-loop system including the tracking error system, controller and observer can be represented as

$$e_i = A_{i0} e_i - B_i \eta_{i2} \quad (\text{B6})$$

$$\dot{\eta}_{p_{o_i}} = \frac{1}{\varepsilon_i} A_{p_{o_i}} \eta_{p_{o_i}} + B_{p_{o_i}} \dot{\psi}_i \quad (\text{B7})$$

Assumption B: The perturbation  $\Psi_i$  and its derivative  $\dot{\Psi}_i$  are Lipschitz in their arguments and bounded over the domain of interest. In addition,  $\Psi(0) = 0$  and  $\dot{\Psi}(0) = 0$ .

Let us consider  $V_i(e, \eta) = V_{i0}(e_i) + W_i(\eta_i)$  as a Lyapunov function candidate for subsystem (B6) and (B7), where

$$V_{i0}(e_i) = e_i^T P_{i1} e_i$$

over a ball  $B(0, o_i) \subset R^3$ , for some  $o_i > 0$ , and  $P_{i1}$  is the positive definite solution of the Lyapunov equation  $P_{i1} A_{i0} + A_{i0}^T P_{i1} = -I_{i1}$ , and

$$W_i(\eta_i) = \eta_{p_{o_i}}^T P_{i2} \eta_{p_{o_i}}$$

where  $P_{i2}$  is the positive definite solution of the Lyapunov equation  $P_{i2} A_{p_{o_i}} + A_{p_{o_i}}^T P_{i2} = -I_{i2}$ .

Choose  $\xi_i < o_i$ ; then, given Assumption B, we have,  $\forall (e_i, \eta_{p_{o_i}}) \in B(0, \xi_i) \times \{\|\eta_{p_{o_i}}\| \leq \xi_i\} = \Lambda_i$

$$\left| \dot{\Psi}_i(e_i, \eta_{p_{o_i}}) \right| \leq \gamma_{i2} \quad (\text{B8})$$

where  $\gamma_{i2}$  is an upperbound of  $\dot{\Psi}$ . It can be shown that,  $\forall (e_i, \eta_{p_{o_i}}) \in \Lambda_i$ , then, we have

$$\begin{aligned} \dot{V}_i &= \frac{\partial V_{i0}}{\partial x_i} (A_{i0}x + B_i \eta_{i2}) \\ &\quad + \frac{\partial W_i}{\partial \eta_i} \left( \frac{1}{\varepsilon_i} A_{p_{o_i}} \eta_{p_{o_i}} + B_{p_{o_i}} \dot{\psi}_i \right) \\ &= -\|e_i\|^2 + 2e_i^T P_{i1} B_i \eta_{i2} - \frac{1}{\varepsilon_i} \|\eta_{p_{o_i}}\|^2 \\ &\quad + 2\eta_{p_{o_i}}^T P_{i2} B_{p_{o_i}} \dot{\Psi} \\ &\leq -\|e_i\|^2 - \frac{1}{\varepsilon_i} \|\eta_{p_{o_i}}\|^2 + 2\|P_{i1}\| \|e_i\| \|\eta_{p_{o_i}}\| \\ &\quad + 2\gamma_{i2} \|P_{i2}\| \|\eta_{p_{o_i}}\| \\ &\leq -\|e_i\| (\|e_i\| - 2\|P_{i1}\| \|\eta_{p_{o_i}}\|) \\ &\quad - \|\eta_{p_{o_i}}\| \left( \frac{1}{\varepsilon_i} \|\eta_{p_{o_i}}\| - 2\gamma_{i2} \|P_{i2}\| \right) \end{aligned} \quad (\text{B9})$$

Defining  $\xi_{i2} = 2\varepsilon_i \gamma_{i2} \|P_{i2}\|$  and  $\xi_{i1} = 2\varepsilon_i \|P_{i1}\| \xi_{i2} = 4\varepsilon_i \gamma_{i2} \|P_{i1}\| \|P_{i2}\|$ ; now for any given  $\xi_i \leq o_i$ , we can choose

$$\varepsilon_i^* = \min \left\{ \frac{\xi_i}{8\gamma_{i2} \|P_{i0}\| \|P_{i1}\|}, \frac{\xi_i}{4\gamma_{i2} \|P_{i1}\|} \right\}$$

Then  $\forall \varepsilon_i, 0 < \varepsilon_i < \varepsilon_i^*$ , we have  $\|e_i\| \leq \frac{\xi_i}{2}$ ,  $\|\eta_{p_{o_i}}\| \leq \frac{\xi_i}{2}$ ,  $\|e_i\| \geq \xi_{i1}$ , and  $\|\eta_{p_{o_i}}\| \geq \xi_{i2}$ , such that

$$\dot{V}_i \leq -\|e_i\| (\|e_i\| - \xi_{i1}) - \|\eta_{p_{o_i}}\| (\|\eta_{p_{o_i}}\| - \xi_{i2}) \leq 0$$

Thus, there exists  $T_i(\xi_i)$  and  $T_i > 0$ , it can be shown that

$$\|e_i(t)\| + \|\eta_{p_{o_i}}\| \leq \xi_i \quad \forall t \geq T$$

Note 1: Verification of Assumption B. Based on equation (11) and (16), as all physical variables are continuous and bounded, both perturbation terms  $(\Psi_d, \Psi_q)$  and their derivatives are bounded. Thus Assumption B is satisfied.

Note 2: Note after the linearization of system (17), the zero dynamics of the remained non-linearized system (1) are stable [28].

## REFERENCES

- [1] J.M. Carrasco, L.G. Franquelo, J.T. Bialasiewicz, E. Galvan, R.C. PortilloGuisado, M.A. M. Prats, J.I. Leon, and N. Moreno-Alfonso, "Power-electronic systems for the grid integration of renewable energy sources: A survey," *IEEE Trans. Ind. Electron.*, vol. 53, no. 4, pp. 1002–1016, June 2006.
- [2] B. Shen, B. Mwinyiwiwa, Y. Zhang, and B.T. Ooi, "Sensorless maximum power point tracking of wind by dfig using rotor position phase lock loop (pll)," *IEEE Trans. Power Electron.*, vol. 24, no. 4, pp. 942–951, April 2009.
- [3] G.D. Marques and M.F. Iacchetti, "Stator frequency regulation in a field-oriented controlled dfig connected to a dc link," *IEEE Trans. Ind. Electron.*, vol. 61, no. 11, pp. 5930–5939, Nov 2014.
- [4] G. Tapia, A. Tapia, and J. Ostolaza, "Proportional-integral regulatorbased approach to wind farm reactive power management for secondary voltage control," *IEEE Trans. Energy Conv.*, vol. 22, no. 2, pp. 488–498, June 2007.
- [5] J. Kim, J. K. Seok, E. Muljadi and Y. C. Kang, "Adaptive Q–V Scheme for the Voltage Control of a DFIG-Based Wind Power Plant," in *IEEE Trans. Power Electron.*, vol. 31, no. 5, pp. 3586–3599, May 2016.
- [6] R. Pena, J. Clare, and G. Asher, "Doubly fed induction generator using back-to-back pwm converters and its application to variable-speed windenergy generation," *IEE Proc. Elec. Power Application*, vol. 143, no. 3, pp. 231–241, May 1996.
- [7] M. Yamamoto and O. Motoyoshi, "Active and reactive power control for doubly-fed wound rotor induction generator," *IEEE Trans. Power Electron.*, vol. 6, no. 4, pp. 624–629, Oct 1991.
- [8] A. Petersson, L. Harnefors, and T. Thiringer, "Evaluation of current control methods for wind turbines using doubly-fed induction machines," *IEEE Trans. Power Electron.*, vol. 20, no. 1, pp. 227–235, Jan 2005.
- [9] H. Akagi and H. Sato, "Control and performance of a doubly-fed induction machine intended for a flywheel energy storage system," *IEEE Trans. Power Electron.*, vol. 17, no. 1, pp. 109–116, Jan 2002.
- [10] S. Chondrogiannis and M. Barnes, "Stability of doubly-fed induction generator under stator voltage orientated vector control," *IET Renewable Power Gen.*, vol. 2, no. 3, pp. 170–180, September 2008.
- [11] E. Tremblay, S. Atayde, and A. Chandra, "Comparative study of control strategies for the doubly fed induction generator in wind energy conversion systems: A dsp-based implementation approach," *IEEE Trans. Sustain. Energy*, vol. 2, no. 3, pp. 288–299, July 2011.
- [12] J. F. Hu, J. Zhu, Y. Zhang, G. Platt, Q. Ma and D. G. Dorrell, "Predictive Direct Virtual Torque and Power Control of Doubly Fed Induction Generators for Fast and Smooth Grid Synchronization and Flexible Power Regulation," in *IEEE Trans. Power Electron.*, vol. 28, no. 7, pp. 3182–3194, July 2013.
- [13] D. Zhi, L. Xu and B. W. Williams, "Model-Based Predictive Direct Power Control of Doubly Fed Induction Generators," in *IEEE Trans. Power Electron.*, vol. 25, no. 2, pp. 341–351, Feb. 2010
- [14] J. Hu, H. Nian, B. Hu, Y. He, and Z. Zhu, "Direct active and reactive power regulation of dfig using sliding-mode control approach," *IEEE Trans. Energy Conv.*, vol. 25, no. 4, pp. 1028–1039, Dec 2010.
- [15] A. Feijo, J. Cidrs, and C. Carrillo, "A third order model for the doubly-fed induction machine," *Electric Power Systems Research*, vol. 56, no. 2, pp. 121 –, 2000.
- [16] Y. Lei, A. Mullane, G. Lightbody, and R. Yacamini, "Modeling of the wind turbine with a doubly fed induction generator for grid integration studies," *IEEE Trans. Energy Conv.*, vol. 21, no. 1, pp. 257–264, March 2006.
- [17] J. Ekanayake, L. Holdsworth, and N. Jenkins, "Comparison of 5<sup>th</sup> order and 3<sup>rd</sup> order machine models for doubly fed induction generator (dfig) wind turbines," *Electric Power Systems Research*, vol. 67, no. 3, pp. 207 – 215, 2003.
- [18] S. Hu, X. Lin, Y. Kang and X. Zou, "An Improved Low-Voltage Ride-Through Control Strategy of Doubly Fed Induction Generator During Grid Faults," in *IEEE Trans. on Power Electron.*, vol. 26, no. 12, pp. 3653–3665, Dec. 2011.
- [19] H. Chaal and M. Jovanovic, "Toward a Generic Torque and Reactive Power Controller for Doubly Fed Machines," in *IEEE Trans. Power Electron.*, vol. 27, no. 1, pp. 113–121, Jan. 2012.
- [20] H. Nian and Y. Song, "Direct Power Control of Doubly Fed Induction Generator Under Distorted Grid Voltage," in *IEEE Trans. Power Electron.*, vol. 29, no. 2, pp. 894–905, Feb. 2014.
- [21] L. Xu and P. Cartwright, "Direct active and reactive power control of dfig for wind energy generation," *IEEE Trans. Energy Conv.*, vol. 21, no. 3, pp. 750–758, Sept 2006.
- [22] S. Mondal and D. Kastha, "Improved direct torque and reactive power control of a matrix-converter-fed grid-connected doubly fed induction generator," *IEEE Trans. Ind. Electron.*, vol. 62, no. 12, pp. 7590–7598, Dec 2015
- [23] P. Xiong and D. Sun, "Backstepping-Based DPC Strategy of a Wind Turbine-Driven DFIG Under Normal and Harmonic Grid Voltage," in *IEEE Trans. Power Electron.*, vol. 31, no. 6, pp. 4216–4225, June 2016.
- [24] G. Rigatos, P. Siano, N. Zervos and C. Cecati, "Control and Disturbances Compensation for Doubly Fed Induction Generators Using the Derivative-Free Nonlinear Kalman Filter," in *IEEE Trans. Power Electron.*, vol. 30, no. 10, pp. 5532–5547, Oct. 2015.
- [25] A. Balogun, O. Ojo and F. Okafor, "Decoupled Direct Control of Natural and Power Variables of Doubly Fed Induction Generator for Extended Wind Speed Range Using Feedback Linearization," in *IEEE Jour. of Emerging and Selected Topics in Power Electron.*, vol. 1, no. 4, pp. 226–237, Dec. 2013.
- [26] M. Mohseni, S. Islam, and M. Masoum, "Enhanced hysteresis-based current regulators in vector control of dfig wind turbines," *IEEE Trans. Power Electron.*, vol. 26, no. 1, pp. 223–234, Jan 2011.
- [27] J. Mohammadi, S. Vaez-Z Adeg, S. Afsharnia, and E. Daryabeigi, "A combined vector and direct power control for dfig-based wind turbines," *IEEE Trans. Sustain. Energy*, vol. 5, no. 3, pp. 767–775, July 2014.
- [28] J. Mauricio, A. Leon, A. Gomez-Exposito, and J. Solsona, "An adaptive nonlinear controller for dfim-based wind energy conversion systems," *IEEE Trans. Energy Conv.*, vol. 23, no. 4, pp. 1025–1035, Dec 2008.
- [29] G. Chen, L. Zhang, X. Cai, W. Zhang, and C. Yin, "Nonlinear control of the doubly fed induction generator by input-output linearizing strategy," in *Electronics and Signal Processing, ser. Lecture Notes in Electrical Engineering*, W. Hu, Ed. Springer Berlin Heidelberg, 2011, pp. 601–608.
- [30] R. Zhu, Z. Chen, Y. Tang, F. Deng, and X. Wu, "Dual-loop control strategy for dfig-based wind turbines under grid voltage disturbances," *IEEE Trans. Power Electron.*, vol. 31, no. 3, pp. 2239–2253, March 2016.
- [31] Q. Huang, X. Zou, D. Zhu and Y. Kang, "Scaled Current Tracking Control for Doubly Fed Induction Generator to Ride-Through Serious Grid Faults," in *IEEE Trans. Power Electron.*, vol. 31, no. 3, pp. 2150–2165, March 2016.
- [32] M. Mohseni and S. M. Islam, "Transient Control of DFIG-Based Wind Power Plants in Compliance With the Australian Grid Code," in *IEEE Trans. Power Electron.*, vol. 27, no. 6, pp. 2813–2824, June 2012

- [33] H. Geng, C. Liu and G. Yang, "LVRT Capability of DFIG-Based WECS Under Asymmetrical Grid Fault Condition," in *IEEE Trans. Ind. Electron.*, vol. 60, no. 6, pp. 2495-2509, June 2013.
- [34] Z. Xie, X. Zhang, X. Zhang, S. Yang and L. Wang, "Improved Ride-Through Control of DFIG During Grid Voltage Swell," in *IEEE Trans. Ind. Electron.*, vol. 62, no. 6, pp. 3584-3594, June 2015.
- [35] W. Chen, D. Xu, N. Zhu, M. Chen and F. Blaabjerg, "Control of Doubly-Fed Induction Generator to Ride-Through Recurring Grid Faults," in *IEEE Trans. Power Electron.*, vol. 31, no. 7, pp. 4831-4846, July 2016.
- [36] J. P. da Costa, H. Pinheiro, T. Degner and G. Arnold, "Robust Controller for DFIGs of Grid-Connected Wind Turbines," in *IEEE Trans. Ind. Electron.*, vol. 58, no. 9, pp. 4023-4038, Sept. 2011.
- [37] J.-J. E. Slotine and W. Li, *Applied Nonlinear Control*. Upper Saddle River, New Jersey: Prentice Hall, 1991.
- [38] W. H. Chen, J. Yang, L. Guo and S. Li, "Disturbance-Observer-Based Control and Related Methods—An Overview," in *IEEE Transactions on Industrial Electronics*, vol. 63, no. 2, pp. 1083-1095, Feb. 2016.
- [39] L. Jiang, Q. Wu, and J. Wen, "Decentralized nonlinear adaptive control for multi-machine power systems via high-gain perturbation observer," *IEEE Trans. Circuits. and Sys. I*, vol. 51, no. 10, pp. 2052–2059, Oct 2004.
- [40] Y. Liu, Q. H. Wu, X. X. Zhou and L. Jiang, "Perturbation Observer Based Multiloop Control for the DFIG-WT in Multimachine Power System," in *IEEE Transactions on Power Systems*, vol. 29, no. 6, pp. 2905-2915, Nov. 2014.
- [41] R. Cardenas, R. Pena, S. Alepuz, and G. Asher, "Overview of control systems for the operation of dfigs in wind energy applications," *IEEE Trans. Ind. Electron.*, vol. 60, no. 7, pp. 2776–2798, July 2013.
- [42] A. Tapia, G. Tapia, J. X. Ostolaza and J. R. Saenz, "Modeling and control of a wind turbine driven doubly fed induction generator," in *IEEE Transactions on Energy Conversion*, vol. 18, no. 2, pp. 194-204, June 2003.
- [43] J. Sloopweg, S. de Haan, H. Polinder, and W. Kling, "General model for representing variable speed wind turbines in power system dynamics simulations," *IEEE Trans. Power Sys.*, vol. 18, no. 1, pp. 144–151, Feb 2003.
- [44] S. Li, T. Haskew, K. Williams, and R. Swatloski, "Control of dfig wind turbine with direct-current vector control configuration," *IEEE Trans. Sustain. Energy*, vol. 3, no. 1, pp. 1–11, Jan 2012.
- [45] Wen-Hua Chen, D. J. Ballance, P. J. Gawthrop and J. O'Reilly, "A nonlinear disturbance observer for robotic manipulators," in *IEEE Transactions on Industrial Electronics*, vol. 47, no. 4, pp. 932-938, Aug 2000.
- [46] Gonzalo Abad; Jesús López; Miguel Rodríguez; Luis Marroyo; Grzegorz Iwanski, *Doubly Fed Induction Machine: Modeling and Control for Wind Energy Generation Applications*, 1, Wiley-IEEE Press, 2011
- [47] J. Kim, J. K. Seok, E. Muljadi and Y. C. Kang, "Adaptive Q–V Scheme for the Voltage Control of a DFIG-Based Wind Power Plant," in *IEEE Transactions on Power Electronics*, vol. 31, no. 5, pp. 3586-3599, May 2016.
- [48] H.K. Khalil, *Nonlinear Systems*, Prentice Hall, 2002.
- [49] Dawei Xiang, Li Ran, P. J. Tavner and S. Yang, "Control of a doubly fed induction generator in a wind turbine during grid fault ride-through," in *IEEE Transactions on Energy Conversion*, vol. 21, no. 3, pp. 652-662, Sept. 2006.